Multibody System Dynamics
https://doi.org/10.1007/s11044-025-10054-4

RESEARCH

Fluid-conveying pipes in the floating frame of reference formulation

Karlijn van Voorthuizen[1] · Mohammed Iqbal Abdul Rasheed[1] · Jurnan Schilder[1]

Received: 8 April 2024 / Accepted: 19 January 2025

Abstract
This work presents a new formulation for flexible fluid-conveying pipe elements based on the widely used floating frame of reference formulation. The elements can be used as a tool for the analysis of flexible multibody systems that contain fluid-conveying pipes, as it is well known that the movement of the fluid can influence the behavior and stability of such systems. The pipe defines a control volume through which the fluid, which is considered to be a moving mass, axially flows. The velocity of a material point of the fluid is therefore a material derivative of its position, representing the large rigid movement and small elastic deformation of the pipe along with the velocity of the fluid with respect to the pipe. The equations of motion are derived through the principle of virtual work, spatial discretization by finite element interpolation functions, and model reduction. A simplification of the consistent equations of motion is proposed, which avoids the use of inertia shape integrals and reduces the effort required to implement the developed fluid-conveying pipe elements in existing multibody software. The developed elements are validated by simulation of a straight cantilevered pipe and a curved pipe constrained on one end by a hinge. A simulation of a concrete printing system illustrates the straightforward incorporation of the elements in larger multibody systems.

Keywords Flexible multibody dynamics · Floating frame of reference formulation · Fluid-conveying pipes · Slender pipe element

1 Introduction

Fluid-conveying pipes are present in many engineering applications ranging from heat exchangers, nuclear reactors, and the chemical and aerospace industry to biological systems and fluidics on micro- and nanoscale [1–4]. As pipes can be subject to rich dynamics or

✉ K. van Voorthuizen
k.l.vanvoorthuizen@utwente.nl

M.I. Abdul Rasheed
m.i.abdulrasheed@utwente.nl

J. Schilder
j.p.schilder@utwente.nl

[1] Faculty of Engineering Technology, University of Twente, P.O. Box 217, 7500 AE Enschede, The Netherlands

Published online: 29 January 2025

even instable behavior introduced by the transported fluid, understanding and predicting the flow induced dynamic behavior of slender pipes has been the subject of many studies [1]. However, typically pipes are not isolated elements but part of larger systems. Many such structures can be considered as multibody systems, as they consist of multiple components connected through joints. Consider, for instance, heavy machinery, exoskeletons, coriolis mass flow meters, and printing robots [5–7]. The dynamic behavior of the flexible pipes may influence the functionality of the complete system and cause unforeseen damage [2, 7, 8]. Therefore modeling of mechanical multibody systems in combination with fluid-conveying pipes to examine the influence of flow-induced behavior is instrumental for the design and functionality of such systems.

Flexible multibody dynamic systems contain components of complex geometries, which can describe large rigid rotations with respect to each other and undergo small elastic deformations. An often employed formulation to describe such systems is the floating frame of reference formulation (FFRF), which is thoroughly discussed in the literature [9]. In this formulation a floating frame is defined for each body in the system. As the floating frame remains close to its related body, the motion of this frame can be considered as the body's gross motion. Elastic deformation is described locally, relative to the floating frame. As the elastic component remains small, a linear finite element model of the bodies can be used to obtain system matrices, and model order reduction techniques can be employed to define the elastic deformation as a truncated superposition of mode shapes, reducing the size of the model. Often used reduction techniques are eigenmode decomposition for different boundary conditions, as, for example, discussed in [10], and component mode synthesis methods such as the Craig–Bampton [11], Herting [12], and Rubin [13] techniques. The kinematic constraints imposed between bodies must be enforced in the constrained equations of motion by the use of Lagrange multipliers, as the constraints are complex expressions in terms of the floating frame coordinates and the modal coordinates. Although enforcing kinematic constraints in the FFRF are typically more complicated compared to alternative formulations, such as nonlinear finite element formulations [14, 15] and corotational formulations [16], the number of degrees of freedom needed to describe the problem is typically smaller. As such, the FFRF is a frequently used description for multibody systems that undergo small elastic deformations [17].

The modeling of the dynamic behavior of fluid-conveying pipes has received considerable interest for many years as well. Reviews of research concerning fluid-conveying pipes such as [1, 18] discuss the dynamic behavior, instabilities, and nonlinear behavior of fluid-conveying pipe systems. More recently, a growing body of research is concerned with the development of nonlinear and geometrically exact formulations of pipes conveying fluid. This includes, among others, development of a geometrically exact theory based on the total momentum of the fluid and the pipe [5], the establishment of a high-dimensional geometrically exact model using Hamilton's principle and Galerkin modal decomposition to investigate the dynamic behavior of a vertical cantilevered fluid-conveying pipe with concentrated mass at the free end [19], and the development of a geometrically exact model for pipes with arbitrary initial configuration [20]. Furthermore, integration of fluid-conveying pipes within multibody systems has gained traction for the finite element-based absolute nodal coordinate formulation (ANCF). Strangl [21] developed a formulation of fluid-conveying pipes in the ANCF for planar systems, whereas Meijaard [6] presented a three-dimensional formulation. Furthermore, Pieper et al. [22] developed an arbitrary Euleria–Lagrangian formulation for fluid-conveying pipes and axially moving beams based on ANCF. Pipe models with the ANCF have been further extended to, for example, the investigation of rotating cantilevered pipes [3] and pipes of various initial configurations [2, 23].

Although integration of fluid-conveying pipes in multibody systems is being carried out for the ANCF, fluid-conveying pipe elements have not been developed within the FFRF. Development of such elements would allow for the analysis of multibody systems modeled in the FFRF, which include fluid-conveying pipes within one framework. Such elements would allow for easy application of existing modeling and analysis tools developed for the FFRF on the combined system. Therefore this paper focuses on the development of fluid-conveying pipe elements within the FFRF.

The method developed in this paper defines the pipe as a control volume for the fluid. The fluid is assumed to be incompressible and inviscid and to move as a plug flow through the pipe with a prescribed velocity and acceleration. As a result, the kinematics of the fluid is expressed through a material derivative that contains both the velocity of a material point of the pipe and the relative velocity of the fluid with respect to pipe along its centerline. Through the principle of virtual work and discretization by the finite element interpolation functions, the mass matrix and quadratic velocity terms of the fluid and the pipe are obtained. Model order reduction of the derived equations of motion for the fluid-conveying pipe is discussed as well. The constraints imposed on the fluid-conveying pipes are expressed with Lagrange multipliers and can be used to constrain the fluid-conveying pipes to elements of various types.

As the derived equations of motion are based on a consistent approach, the mass matrix and the quadratic velocity terms contain inertia shape integrals. Such volume integrals are also found when deriving solid elements based on a consistent approach. Implementations of the FFRF either compute the inertia shape integrals or approximate them using the finite element mass matrix. As the mass matrix and quadratic velocity terms of the fluid-conveying pipe element contain volume integrals, which do not appear for solid elements, this work considers an approximation of the fluid-conveying pipe element based on its finite element model. In this way, exact calculation of the inertia shape integrals unique to the fluid-conveying pipe elements is avoided. The element matrices of a pipe of arbitrary shape are approximated by preimposing deformation upon a straight pipe and ensuring that the initial state corresponds with the desired stress state. To ensure that the deformation in a pipe body remains small, it may be necessary to use multiple bodies to simulate a pipe of large curvature. This section finalizes with a discussion on how to efficiently incorporate the simplified flexible fluid-conveying pipes into existing software packages.

This paper is structured as follows. The first part of the work is focused on defining the equations of motion for a single element of the fluid conveying pipe. To this end, the kinematics of the pipe and the fluid are described in Sect. 2, the principle of virtual work is used to derive the mass and quadratic velocity terms in Sect. 3, and spacial discretization by finite element interpolation functions to define the internal behavior of the element is discussed in Sect. 4. Section 5 shows the assembly of multiple elements into a body of the fluid-conveying pipe, followed by a discussion on model order reduction. The constrained equations of motion are formulated in Sect. 6. A simplification of the derived equations of motion is proposed in Sect. 7. The developed formulation is validated in Sect. 8 through comparison of the results of an implementation of the developed elements on the problem of a cantilevered straight pipe and a rotating semicircular pipe with the established ANCF fluid-conveying pipes [6] implemented within Spacar [24]. Furthermore, a simplified concrete printing robot is modeled to illustrate how the fluid-conveying pipe elements can be used in conjunction with solid elements.

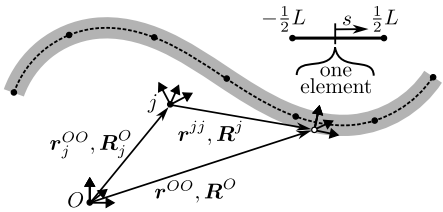

Fig. 1 A schematic illustration of the coordinates used to define the kinematics of the fluid-conveying pipe

2 Kinematics

Consider a pipe with a three-dimensional centerline of arbitrary shape as illustrated in Fig. 1. The pipe consists of multiple elements with a node at either end of each element. In Fig. 1, this is indicated by the circles along the centerline of the pipe. For each element, a local coordinate s is defined along its centerline in the undeformed configuration such that $-\frac{1}{2}L \leq s \leq \frac{1}{2}L$, with L denoting the length of the undeformed element along the centerline. In the first part of this work, the focus is on deriving the equations of motion of a single pipe element. Once this has been achieved, assembly of elements will be discussed.

The kinematics of the pipe element is described with respect to the global coordinate system with its origin in point O, as shown in Fig. 1. This coordinate system is further referred to as the *global frame*. Consider a material point of the pipe element to which a frame is rigidly attached, as illustrated by the white circle in Fig. 1. The position of the frame attached to the material point with respect to the global frame O is denoted by the position vector $\boldsymbol{r}^{OO}$. The index notation of this position vector must be read as the position of the material point relative to the global frame (second superscript) expressed in the global frame (first superscript). The orientation of the frame attached to the material point with respect to the global frame O is denoted by the rotation matrix $\boldsymbol{R}^O$. The index notion of the rotation matrix must be read as the orientation of the frame attached to the material point relative to the global frame (superscript).

The pipe element may describe a rigid-body motion with respect to the global frame and experience elastic deformation. The rigid-body motion can be described by the trajectory of a floating frame of reference, referred to as the *floating frame*. One floating frame can be used to describe the rigid motion of multiple elements. The collection of one or more elements for which a single floating frame is defined is referred to as a *body*. Let the floating frame be denoted by j. The position of the material point can be expressed as a function of the global position vector of the floating frame $\boldsymbol{r}_j^{OO}$ and the local position vector of the material point $\boldsymbol{r}^{jj}$, i.e.,

$$\boldsymbol{r}^{OO}(t,s) = \boldsymbol{r}_j^{OO}(t) + \boldsymbol{r}^{Oj}(t,s) = \boldsymbol{r}_j^{OO}(t) + \boldsymbol{R}_j^O(t)\boldsymbol{r}^{jj}(t,s), \tag{1}$$

where $\boldsymbol{R}_j^O$ denotes the rotation matrix expressing the orientation of the floating frame relative to the global frame, and the terms between brackets denote the dependency on time t and the local centerline coordinate. Note that the subscripts of the position vector and the rotation matrix denote the node for which the position or orientation is being described. If the subscript is omitted, then the position or orientation of the frame attached to an arbitrary material point is considered. The local position vector $\boldsymbol{r}^{jj}$ can be decomposed as the sum of the position of the material point on the undeformed body $\boldsymbol{x}^{jj}$ and the elastic deformation $\boldsymbol{u}^{jj}$:

$$\boldsymbol{r}^{jj}(t,s) = \boldsymbol{x}^{jj}(s) + \boldsymbol{u}^{jj}(t,s). \tag{2}$$

Substitution of Eq. (2) in Eq. (1) yields

$$\boldsymbol{r}^{OO}(t,s) = \boldsymbol{r}_j^{OO}(t) + \boldsymbol{R}_j^O(t)(\boldsymbol{x}^{jj}(s) + \boldsymbol{u}^{jj}(t,s)). \tag{3}$$

The rotation matrix, which expresses the orientation of the frame attached to the material point relative to the global frame $\boldsymbol{R}^O$, can be expressed using the floating frame as well:

$$\boldsymbol{R}^O(t,s) = \boldsymbol{R}_j^O(t)\boldsymbol{R}^j(t,s), \tag{4}$$

where $\boldsymbol{R}^j$ is the rotation matrix that expresses the orientation of the frame attached to the material point relative to the floating frame. This is schematically illustrated in Fig. 1. In the following sections the explicit notation indicating time dependency and dependence on s is omitted for clarity.

2.1 A note on the angular parameterization

The rotation matrix is a proper orthogonal matrix that satisfies

$$\boldsymbol{R}_j^O \boldsymbol{R}_O^j = \mathbf{1} \tag{5}$$

with $\mathbf{1}$ denoting the identity matrix, and

$$(\boldsymbol{R}_j^O)^{-1} = (\boldsymbol{R}_j^O)^T = \boldsymbol{R}_O^j. \tag{6}$$

As such, the time derivative of the rotation matrix can be written as

$$\dot{\boldsymbol{R}}_j^O = \tilde{\boldsymbol{\omega}}_j^{OO}\boldsymbol{R}_j^O, \tag{7}$$

where $\tilde{\boldsymbol{\omega}}_j^{OO}$ is the skew symmetric representation of $\boldsymbol{\omega}_j^{OO}$, which is the vector of angular velocities of the floating frame relative to the global frame, and the dot is used to represent the partial derivative with respect to time, $\dot{(\bullet)} = \frac{\partial(\bullet)}{\partial t}$.

A rotation matrix can be defined using different angular parameterizations, such as Euler parameters, Euler angles, Rodriguez parameters, and so on. Let the vector of rotational coordinates that define the rotation matrix be denoted as $\boldsymbol{p}$, so that $\boldsymbol{R} = \boldsymbol{R}(\boldsymbol{p})$. Irrespective of the angular parameterization, the relation between the angular velocities $\boldsymbol{\omega}$ and the rotational coordinates can be expressed as

$$\boldsymbol{\omega} = \boldsymbol{G}(\boldsymbol{p})\dot{\boldsymbol{p}}, \tag{8}$$

where the matrix $\boldsymbol{G}(\boldsymbol{p})$ is defined by the chosen angular parameterization. The angular accelerations are expressed in terms of the rotational coordinates as

$$\dot{\boldsymbol{\omega}} = \boldsymbol{G}(\boldsymbol{p})\ddot{\boldsymbol{p}} + \dot{\boldsymbol{G}}(\boldsymbol{p})\dot{\boldsymbol{p}}, \tag{9}$$

and the variation of the angular displacements $\delta\boldsymbol{\pi}$, also referred to as virtual rotations, as

$$\delta\boldsymbol{\pi} = \boldsymbol{G}(\boldsymbol{p})\delta\boldsymbol{p}. \tag{10}$$

The derivation of the fluid-conveying pipe elements will be performed in terms of the variation of the angular displacements, angular velocities, and angular accelerations, without assuming a specific angular parameterization. As a result, the derived pipe elements can be implemented using any parameterization of choice by utilizing Eqs. (8), (9), and (10).

2.2 Velocities and accelerations of the pipe

Let us consider the velocity and acceleration of a material point of the pipe element. Time differentiation of Eq. (3) yields the global velocity of the material point of the pipe, which, using Eq. (7), can be written as

$$\dot{\boldsymbol{r}}^{OO} = \begin{bmatrix} \mathbf{1} & \boldsymbol{R}_j^O(\tilde{\boldsymbol{r}}^{jj})^T \boldsymbol{R}_O^j & \boldsymbol{R}_j^O \end{bmatrix} \begin{bmatrix} \dot{\boldsymbol{r}}_j^{OO} \\ \boldsymbol{\omega}_j^{OO} \\ \dot{\boldsymbol{u}}^{jj} \end{bmatrix}. \tag{11}$$

Time differentiation of Eq. (11) yields the accelerations of the material point:

$$\begin{aligned} \ddot{\boldsymbol{r}}^{OO} = & \begin{bmatrix} \mathbf{1} & \boldsymbol{R}_j^O(\tilde{\boldsymbol{r}}^{jj})^T \boldsymbol{R}_O^j & \boldsymbol{R}_j^O \end{bmatrix} \begin{bmatrix} \ddot{\boldsymbol{r}}_j^{OO} \\ \dot{\boldsymbol{\omega}}_j^{OO} \\ \ddot{\boldsymbol{u}}^{jj} \end{bmatrix} \\ & + \begin{bmatrix} \mathbf{0} & \boldsymbol{R}_j^O \tilde{\boldsymbol{\omega}}_j^{jO}(\tilde{\boldsymbol{r}}^{jj})^T \boldsymbol{R}_O^j & 2\boldsymbol{R}_j^O \tilde{\boldsymbol{\omega}}_j^{jO} \end{bmatrix} \begin{bmatrix} \dot{\boldsymbol{r}}_j^{OO} \\ \boldsymbol{\omega}_j^{OO} \\ \dot{\boldsymbol{u}}^{jj} \end{bmatrix}. \end{aligned} \tag{12}$$

2.3 Velocities and accelerations of the fluid

The fluid is assumed to be incompressible and inviscid and moves through the pipe in plug flow. As such, the velocity and acceleration of the fluid with respect to the pipe in the direction of the centerline are homogeneous throughout the pipe. To obtain an equation of motion that describes the behavior of the fluid-conveying pipe, only the fluid located in the pipe at any time is of interest. As such, the pipe represents a control volume through which the material points of the fluid are axially moving. The material domain of the pipe can therefore be used as a nonmaterial domain to describe the behavior of the fluid [25]. Consequently, the expression for the position of a material point of the pipe (Eq. (3)) can also be used to describe the position of a material point of the fluid. However, to obtain the velocities and accelerations of the fluid, the material derivative

$$\frac{d\boldsymbol{r}^{OO}}{dt} = \frac{\partial \boldsymbol{r}^{OO}}{\partial t} + \frac{\partial \boldsymbol{r}^{OO}}{\partial s}\frac{\partial s}{\partial t} \tag{13}$$

must be utilized as the local centerline coordinate corresponding to a material point of the fluid is time dependent. The short hand $(\bullet)' = \frac{\partial(\bullet)}{\partial s}$ further denotes the partial derivative with respect to s, so that

$$\frac{d\boldsymbol{r}^{OO}}{dt} = \dot{\boldsymbol{r}}^{OO} + (\boldsymbol{r}^{OO})'\dot{s}. \tag{14}$$

Here $\frac{d\boldsymbol{r}^{OO}}{dt}$ represents the total velocity of a material point of the fluid with respect to the global frame. Furthermore, $\dot{\boldsymbol{r}}^{OO}$ denotes the change in the position of the control volume, the pipe, in time. Finally, $\dot{s}$ represents the relative velocity of the fluid with respect to the pipe in the direction of the centerline of the pipe, and $(\boldsymbol{r}^{OO})'$ represents the orientation of

the centerline at a material point of the fluid with respect to the global frame. As the local centerline coordinate s is defined in the undeformed configuration and the pipe can elongate, the length of the vector $(\boldsymbol{r}^{OO})'$ does not necessarily equal one. In fact, to obtain Eq. (14), it is assumed that the derivative of the local centerline coordinate in the undeformed configuration (s) with respect to the local centerline coordinate in the deformed configuration (s_{def}) approximately equals one,

$$\frac{\partial s}{\partial s_{\text{def}}} \approx 1, \tag{15}$$

where $-\frac{1}{2}L_{\text{def}} \leq s_{\text{def}} \leq \frac{1}{2}L_{\text{def}}$ with L_{def} denoting the length of the deformed element along the centerline. The assumption shown in Eq. (15) is valid if the elongation of the pipe remains small and, under these circumstances, introduces only small errors in the magnitude of the inertia forces for the fluid. Finally, note that $\dot{s}$ has the same value throughout the cross-section as well as the length of the pipe due to the assumption of incompressibility and plug flow. Consequently, $\dot{s}' = 0$. This value can however change over time, meaning that the acceleration $\ddot{s}$ does not necessarily equal zero but does again have the same value throughout the cross-section and length of the pipe.

Let us consider the term $(\boldsymbol{r}^{OO})'$ in more detail. Equation (3) expresses $\boldsymbol{r}^{OO}$ using the floating frame:

$$(\boldsymbol{r}^{OO})' = (\boldsymbol{r}_j^{OO} + \boldsymbol{R}_j^O \boldsymbol{r}^{jj})'. \tag{16}$$

As the position and orientation of the floating frame is independent of the centerline coordinate corresponding to the material point, Eq. (16) can be written as

$$(\boldsymbol{r}^{OO})' = \boldsymbol{R}_j^O (\boldsymbol{r}^{jj})' = \boldsymbol{R}_j^O (\boldsymbol{x}^{jj} + \boldsymbol{u}^{jj})'. \tag{17}$$

As such, $(\boldsymbol{r}^{jj})'$ expresses, in the coordinate system of the floating frame, the direction of the centerline of the pipe in the deformed configuration. As an illustrative example, consider an element of a rigid straight pipe for which the position of the floating frame coincides with the center of the element and the x-axis of the floating frame coincides with the centerline such that

$$\boldsymbol{r}^{jj} = \boldsymbol{x}^{jj} = \begin{bmatrix} s \\ 0 \\ 0 \end{bmatrix} \quad \text{and} \quad (\boldsymbol{r}^{jj})' = \begin{bmatrix} 1 \\ 0 \\ 0 \end{bmatrix}. \tag{18}$$

Clearly, the product $(\boldsymbol{r}^{jj})'\dot{s}$ specifies that the velocity of the fluid with respect to the pipe ($\dot{s}$) is always in the direction of the x-axis of the floating frame.

Time differentiation of Eq. (3) using Eq. (14) and utilizing the properties of the skew symmetric matrix yield the velocity of a material point of the fluid:

$$\dot{\boldsymbol{r}}^{OO} = \begin{bmatrix} \mathbf{1} & \boldsymbol{R}_j^O (\tilde{\boldsymbol{r}}^{jj})^T \boldsymbol{R}_O^j & \boldsymbol{R}_j^O & \boldsymbol{R}_j^O (\boldsymbol{r}^{jj})' \end{bmatrix} \begin{bmatrix} \dot{\boldsymbol{r}}_j^{OO} \\ \boldsymbol{\omega}_j^{OO} \\ \dot{\boldsymbol{u}}^{jj} \\ \dot{s} \end{bmatrix}. \tag{19}$$

Further differentiation with respect to time allows us to formulate the global accelerations of the material point of the fluid:

$$\ddot{\boldsymbol{r}}^{OO} = \begin{bmatrix} \mathbf{1} & \boldsymbol{R}_j^O(\tilde{\boldsymbol{r}}^{jj})^T \boldsymbol{R}_O^j & \boldsymbol{R}_j^O & \boldsymbol{R}_j^O(\boldsymbol{r}^{jj})' \end{bmatrix} \begin{bmatrix} \ddot{\boldsymbol{r}}_j^{OO} \\ \dot{\boldsymbol{\omega}}_j^{OO} \\ \ddot{\boldsymbol{u}}^{jj} \\ \ddot{s} \end{bmatrix}$$

$$+ \begin{bmatrix} \mathbf{0} & \boldsymbol{R}_j^O\tilde{\boldsymbol{\omega}}_j^{jO}(\tilde{\boldsymbol{r}}^{jj})^T \boldsymbol{R}_O^j & 2\boldsymbol{R}_j^O\tilde{\boldsymbol{\omega}}_j^{jO} & 2\boldsymbol{R}_j^O\tilde{\boldsymbol{\omega}}_j^{jO}(\boldsymbol{r}^{jj})' + 2\boldsymbol{R}_j^O(\dot{\boldsymbol{r}}^{jj})' + \boldsymbol{R}_j^O(\boldsymbol{r}^{jj})''\dot{s} \end{bmatrix} \begin{bmatrix} \dot{\boldsymbol{r}}_j^{OO} \\ \boldsymbol{\omega}_j^{OO} \\ \dot{\boldsymbol{u}}^{jj} \\ \dot{s} \end{bmatrix} \tag{20}$$

The derivatives of the local position vector with respect to s can be decomposed using Eq. (2) as

$$(\boldsymbol{r}^{jj})' = (\boldsymbol{x}^{jj})' + (\boldsymbol{u}^{jj})', \tag{21}$$

$$(\dot{\boldsymbol{r}}^{jj})' = (\dot{\boldsymbol{u}}^{jj})', \quad \text{and} \tag{22}$$

$$(\boldsymbol{r}^{jj})'' = (\boldsymbol{x}^{jj})'' + (\boldsymbol{u}^{jj})'' \tag{23}$$

since the undeformed configuration is time-independent ($\dot{\boldsymbol{x}}^{jj} = \mathbf{0}$).

3 Principle of virtual work

The equations of motion of the flexible fluid-conveying pipe are derived through the principle of virtual work

$$\delta W_{ex} = \delta W_{el,p} + \delta W_{in,p} + \delta W_{in,f}, \tag{24}$$

where W_{ex} denotes the work by external forces, $W_{el,p}$ denotes the work by elastic forces for the pipe, and $W_{in,p}$ and $W_{in,f}$ denote the work by inertia forces for the pipe and the fluid, respectively. Note that using the kinematic relations derived in the previous section, the virtual work terms of the fluid and the pipe can be expressed using the same set of coordinates. As such, the total virtual work due to inertia forces is written as

$$\delta W_{in} = \begin{bmatrix} \delta\boldsymbol{r}_j^{OO} \\ \delta\boldsymbol{\pi}_j^{OO} \\ \delta\boldsymbol{u}^{jj} \\ \delta s \end{bmatrix}^T (\boldsymbol{Q}_{in,p} + \boldsymbol{Q}_{in,f}) \tag{25}$$

with $\boldsymbol{Q}_{in,p}$ and $\boldsymbol{Q}_{in,f}$ being the inertia forces for the pipe and fluid, respectively.

The external virtual work δW_{ex} can be written as

$$\delta W_{ex} = \begin{bmatrix} \delta\boldsymbol{r}_j^{OO} \\ \delta\boldsymbol{\pi}_j^{OO} \\ \delta\boldsymbol{u}^{jj} \\ \delta s \end{bmatrix}^T \begin{bmatrix} \boldsymbol{Q}^O \\ Q_s^O \end{bmatrix}, \tag{26}$$

where $\boldsymbol{Q}^O$ contains the externally applied forces and moments such as body forces or applied forces on the outside of the pipe. As the interface forces between the pipe and fluid do not perform any work, these forces are not included in $\boldsymbol{Q}^O$. For an element with two nodes, $\boldsymbol{Q}^O$ is a vector of dimensions 18×1, and Q_s^O is a scalar, which can be interpreted as the force responsible for the movement of the fluid relative to the pipe.

As the fluid cannot experience elastic forces, the virtual work due to elastic forces is considered for the pipe only. The pipe is considered as a linear elastic solid:

$$\delta W_{el,p} = \int_V (\delta \boldsymbol{\epsilon}^{jj})^T \boldsymbol{\sigma}^{jj} dV, \tag{27}$$

where $\boldsymbol{\epsilon}^{jj}$ and $\boldsymbol{\sigma}^{jj}$ are the internal strains and stresses at a material point for the pipe, and V is the volume.

The virtual work by inertia forces must be considered for both the pipe and fluid. For some material point on the pipe, δW_{in} is expressed as

$$\delta W_{in} = \int_V (\delta \boldsymbol{r}^{OO})^T \ddot{\boldsymbol{r}}^{OO} \rho \, dV, \tag{28}$$

where ρ is the density at the material point. The virtual work by inertia forces for the pipe $\delta W_{in,p}$ is evaluated by substitution of Eq. (11) and Eq. (12) into Eq. (28):

$$\begin{aligned} \delta W_{in,p} = \int_V \begin{bmatrix} \delta \boldsymbol{r}_j^{OO} \\ \delta \boldsymbol{\pi}_j^{OO} \\ \delta \boldsymbol{u}^{jj} \end{bmatrix}^T \Bigg(& \begin{bmatrix} \hat{\boldsymbol{R}}_j^O \end{bmatrix} \begin{bmatrix} \mathbf{1} & (\tilde{\boldsymbol{r}}^{jj})^T & \mathbf{1} \\ \tilde{\boldsymbol{r}}^{jj} & \tilde{\boldsymbol{r}}^{jj} (\tilde{\boldsymbol{r}}^{jj})^T & \tilde{\boldsymbol{r}}^{jj} \\ \mathbf{1} & (\tilde{\boldsymbol{r}}^{jj})^T & \mathbf{1} \end{bmatrix} \begin{bmatrix} \hat{\boldsymbol{R}}_O^j \end{bmatrix} \begin{bmatrix} \ddot{\boldsymbol{r}}_j^{OO} \\ \dot{\boldsymbol{\omega}}_j^{OO} \\ \ddot{\boldsymbol{u}}^{jj} \end{bmatrix} \\ & + \begin{bmatrix} \hat{\boldsymbol{R}}_j^O \end{bmatrix} \begin{bmatrix} \tilde{\boldsymbol{\omega}}_j^{jO} (\tilde{\boldsymbol{r}}^{jj})^T \boldsymbol{\omega}_j^{jO} + 2\tilde{\boldsymbol{\omega}}_j^{jO} \dot{\boldsymbol{u}}^{jj} \\ \tilde{\boldsymbol{r}}^{jj} \tilde{\boldsymbol{\omega}}_j^{jO} (\tilde{\boldsymbol{r}}^{jj})^T \boldsymbol{\omega}_j^{jO} + 2\tilde{\boldsymbol{r}}^{jj} \tilde{\boldsymbol{\omega}}_j^{jO} \dot{\boldsymbol{u}}^{jj} \\ \tilde{\boldsymbol{\omega}}_j^{jO} (\tilde{\boldsymbol{r}}^{jj})^T \boldsymbol{\omega}_j^{jO} + 2\tilde{\boldsymbol{\omega}}_j^{jO} \dot{\boldsymbol{u}}^{jj} \end{bmatrix} \Bigg) \rho_p dV \end{aligned} \tag{29}$$

with

$$\begin{bmatrix} \hat{\boldsymbol{R}}_j^O \end{bmatrix} = \begin{bmatrix} \boldsymbol{R}_j^O & \mathbf{0} & \mathbf{0} \\ \mathbf{0} & \boldsymbol{R}_j^O & \mathbf{0} \\ \mathbf{0} & \mathbf{0} & \mathbf{1} \end{bmatrix} \tag{30}$$

and ρ_p denoting the density of the pipe at the material point. Note that Eq. (29) does not contain a row corresponding to δs. To substitute the virtual work due to inertia forces for the pipe in Eq. (26), a row corresponding to δs that contributes no work should be added.

For the fluid, Eq. (28) provides an approximation of the virtual work by inertia forces, which does not account for the motion of the fluid across the boundary of the control volume [26]. However, since the flow velocity through the pipe is homogenous, the inner diameter of the pipe is constant, and the deformation of the pipe remains small, Eq. (28) is expected to provide a sufficiently accurate approximation. Substitution of Eqs. (19) and (20) into Eq. (28) results in

$$\delta W_{in,f} = \int_V \begin{bmatrix} \delta \boldsymbol{r}_j^{OO} \\ \delta \boldsymbol{\pi}_j^{OO} \\ \delta \boldsymbol{u}^{jj} \\ \delta s \end{bmatrix}^T \left(\begin{bmatrix} \hat{\boldsymbol{R}}_j^O & \mathbf{0} \\ \mathbf{0} & 1 \end{bmatrix} \boldsymbol{A} \begin{bmatrix} \hat{\boldsymbol{R}}_O^j & \mathbf{0} \\ \mathbf{0} & 1 \end{bmatrix} \begin{bmatrix} \ddot{\boldsymbol{r}}_j^{OO} \\ \dot{\boldsymbol{\omega}}_j^{OO} \\ \ddot{\boldsymbol{u}}^{jj} \\ \ddot{s} \end{bmatrix} + \begin{bmatrix} \hat{\boldsymbol{R}}_j^O & \mathbf{0} \\ \mathbf{0} & 1 \end{bmatrix} \boldsymbol{B} \right) \rho_f dV \tag{31}$$

with

$$\boldsymbol{A} = \begin{bmatrix} \mathbf{1} & (\tilde{\boldsymbol{r}}^{jj})^T & \mathbf{1} & (\boldsymbol{r}^{jj})' \\ \tilde{\boldsymbol{r}}^{jj} & \tilde{\boldsymbol{r}}^{jj}(\tilde{\boldsymbol{r}}^{jj})^T & \tilde{\boldsymbol{r}}^{jj} & \tilde{\boldsymbol{r}}^{jj}(\boldsymbol{r}^{jj})' \\ \mathbf{1} & (\tilde{\boldsymbol{r}}^{jj})^T & \mathbf{1} & (\boldsymbol{r}^{jj})' \\ ((\boldsymbol{r}^{jj})')^T & ((\boldsymbol{r}^{jj})')^T(\tilde{\boldsymbol{r}}^{jj})^T & ((\boldsymbol{r}^{jj})')^T & ((\boldsymbol{r}^{jj})')^T(\boldsymbol{r}^{jj})' \end{bmatrix} \tag{32}$$

and

$$\boldsymbol{B} = \begin{bmatrix} \tilde{\boldsymbol{\omega}}_j^{jO}(\tilde{\boldsymbol{r}}^{jj})^T\boldsymbol{\omega}_j^{jO} + 2\tilde{\boldsymbol{\omega}}_j^{jO}\dot{\boldsymbol{u}}^{jj} + \{2\tilde{\boldsymbol{\omega}}_j^{jO}(\boldsymbol{r}^{jj})' + 2(\dot{\boldsymbol{r}}^{jj})' + (\boldsymbol{r}^{jj})''\dot{s}\}\dot{s} \\ \tilde{\boldsymbol{r}}^{jj}\tilde{\boldsymbol{\omega}}_j^{jO}(\tilde{\boldsymbol{r}}^{jj})^T\boldsymbol{\omega}_j^{jO} + 2\tilde{\boldsymbol{r}}^{jj}\tilde{\boldsymbol{\omega}}_j^{jO}\dot{\boldsymbol{u}}^{jj} + \tilde{\boldsymbol{r}}^{jj}\{2\tilde{\boldsymbol{\omega}}_j^{jO}(\boldsymbol{r}^{jj})' + 2(\dot{\boldsymbol{r}}^{jj})' + (\boldsymbol{r}^{jj})''\dot{s}\}\dot{s} \\ \tilde{\boldsymbol{\omega}}_j^{jO}(\tilde{\boldsymbol{r}}^{jj})^T\boldsymbol{\omega}_j^{jO} + 2\tilde{\boldsymbol{\omega}}_j^{jO}\dot{\boldsymbol{u}}^{jj} + \{2\tilde{\boldsymbol{\omega}}_j^{jO}(\boldsymbol{r}^{jj})' + 2(\dot{\boldsymbol{r}}^{jj})' + (\boldsymbol{r}^{jj})''\dot{s}\}\dot{s} \\ ((\boldsymbol{r}^{jj})')^T\tilde{\boldsymbol{\omega}}_j^{jO}(\tilde{\boldsymbol{r}}^{jj})^T\boldsymbol{\omega}_j^{jO} + 2((\boldsymbol{r}^{jj})')^T\tilde{\boldsymbol{\omega}}_j^{jO}\dot{\boldsymbol{u}}^{jj} + ((\boldsymbol{r}^{jj})')^T\{2\tilde{\boldsymbol{\omega}}_j^{jO}(\boldsymbol{r}^{jj})' + 2(\dot{\boldsymbol{r}}^{jj})' + (\boldsymbol{r}^{jj})''\dot{s}\}\dot{s} \end{bmatrix}, \tag{33}$$

ρ_f being the density of the fluid at the material point. Note that as the axial velocity $\dot{s}$ and acceleration $\ddot{s}$ of the fluid are homogeneous throughout the pipe, they can be taken outside the volume integral.

4 Spatial discretization

To compute the volume integrals in the expressions for the virtual work by elastic forces (Eq. (27)) and inertia forces (Eqs. (29) and (31)), the element is discretized by finite element interpolation functions $\boldsymbol{N}(\boldsymbol{x}^{jj})$. As such, the elastic deformation within one element can be expressed as

$$\boldsymbol{u}^{jj}(\boldsymbol{x}^{jj}, t) = \boldsymbol{N}(\boldsymbol{x}^{jj})\bar{\boldsymbol{u}}_{n_{el}}^{jj}(t) \tag{34}$$

with $\bar{\boldsymbol{u}}_{n_{el}}^{jj}(t)$ being the vector of nodal displacements at all the nodes of the element (n_{el}). For an element with two nodes, $\bar{\boldsymbol{u}}_{n_{el}}^{jj}(t)$ is a vector of dimensions 12×1. Note that although $\bar{\boldsymbol{u}}_{n_{el}}^{jj}(t)$ is referred to as the vector of nodal displacements, it contains both displacements and rotations. If an isoparametric element is considered, then the local position vector of the undeformed body of one element can be expressed using the interpolation functions as

$$\boldsymbol{x}^{jj} = \boldsymbol{N}(\boldsymbol{x}^{jj})\bar{\boldsymbol{x}}_{n_{el}}^{jj} \tag{35}$$

with $\bar{\boldsymbol{x}}_{n_{el}}^{jj}$ being the vector containing the local position and orientation of the nodes of the element in the undeformed configuration. For an element with two nodes, $\bar{\boldsymbol{x}}_{n_{el}}^{jj}$ is a vector of dimensions 12×1. Equations (34) and (35) allow us to write the local position vector $\boldsymbol{r}^{jj}$ as

$$\boldsymbol{r}^{jj}(\boldsymbol{x}^{jj}, t) = \boldsymbol{N}(\boldsymbol{x}^{jj})\left(\bar{\boldsymbol{x}}_{n_{el}}^{jj} + \bar{\boldsymbol{u}}_{n_{el}}^{jj}(t)\right). \tag{36}$$

Therefore the following equations must hold for the spatial and time derivatives of the local position vector defined in Eqs. (21), (22), and (23):

$$(\boldsymbol{r}^{jj}(\boldsymbol{x}^{jj}, t))' = \boldsymbol{N}'(\boldsymbol{x}^{jj})\left(\bar{\boldsymbol{x}}_{n_{el}}^{jj} + \bar{\boldsymbol{u}}_{n_{el}}^{jj}(t)\right), \tag{37}$$

$$(\dot{\boldsymbol{r}}^{jj}(\boldsymbol{x}^{jj}, t))' = \boldsymbol{N}'(\boldsymbol{x}^{jj})\dot{\bar{\boldsymbol{u}}}_{n_{el}}^{jj}(t), \tag{38}$$

$$(\boldsymbol{r}^{jj}(\boldsymbol{x}^{jj}, t))'' = \boldsymbol{N}''(\boldsymbol{x}^{jj})\left(\bar{\boldsymbol{x}}_{n_{el}}^{jj} + \bar{\boldsymbol{u}}_{n_{el}}^{jj}(t)\right). \tag{39}$$

After substitution of Eq. (34), the virtual work by elastic forces (Eq. (27)) is expressed as

$$\delta W_{el,p} = (\delta \bar{\boldsymbol{u}}^{jj}_{n_{el}})^T \boldsymbol{K}^j_{p,el} \bar{\boldsymbol{u}}^{jj}_{n_{el}}, \tag{40}$$

where $\boldsymbol{K}^j_{p,el}$ denotes the local finite element stiffness matrix of one pipe element. Substitution of Eq. (34) allows us to write the virtual work by inertia forces for the pipe shown in Eq. (29) as

$$\delta W_{in,p} = \begin{bmatrix} \delta \boldsymbol{r}^{OO}_j \\ \delta \boldsymbol{\pi}^{OO}_j \\ \delta \bar{\boldsymbol{u}}^{jj}_{n_{el}} \end{bmatrix}^T \begin{bmatrix} \hat{\boldsymbol{R}}^O_j \end{bmatrix} \left(\boldsymbol{M}^j_{p,el} \begin{bmatrix} \hat{\boldsymbol{R}}^j_O \end{bmatrix} \begin{bmatrix} \ddot{\boldsymbol{r}}^{OO}_j \\ \dot{\boldsymbol{\omega}}^{OO}_j \\ \ddot{\bar{\boldsymbol{u}}}^{jj}_{n_{el}} \end{bmatrix} + \boldsymbol{D}^j_{p,el} \right) \tag{41}$$

with the element mass matrix of the pipe

$$\boldsymbol{M}^j_{p,el} = \int_V \begin{bmatrix} \boldsymbol{1} & (\tilde{\boldsymbol{r}}^{jj})^T & \boldsymbol{N} \\ \tilde{\boldsymbol{r}}^{jj} & \tilde{\boldsymbol{r}}^{jj}(\tilde{\boldsymbol{r}}^{jj})^T & \tilde{\boldsymbol{r}}^{jj}\boldsymbol{N} \\ \boldsymbol{N}^T & \boldsymbol{N}^T(\tilde{\boldsymbol{r}}^{jj})^T & \boldsymbol{N}^T\boldsymbol{N} \end{bmatrix} \rho_p dV \tag{42}$$

and the quadratic velocity terms for a pipe element

$$\boldsymbol{D}^j_{p,el} = \int_V \begin{bmatrix} \tilde{\boldsymbol{\omega}}^{jO}_j (\tilde{\boldsymbol{r}}^{jj})^T \boldsymbol{\omega}^{jO}_j + 2\tilde{\boldsymbol{\omega}}^{jO}_j \boldsymbol{N} \dot{\bar{\boldsymbol{u}}}^{jj}_{n_{el}} \\ \tilde{\boldsymbol{r}}^{jj} \tilde{\boldsymbol{\omega}}^{jO}_j (\tilde{\boldsymbol{r}}^{jj})^T \boldsymbol{\omega}^{jO}_j + 2\tilde{\boldsymbol{r}}^{jj} \tilde{\boldsymbol{\omega}}^{jO}_j \boldsymbol{N} \dot{\bar{\boldsymbol{u}}}^{jj}_{n_{el}} \\ \boldsymbol{N}^T \tilde{\boldsymbol{\omega}}^{jO}_j (\tilde{\boldsymbol{r}}^{jj})^T \boldsymbol{\omega}^{jO}_j + 2\boldsymbol{N}^T \tilde{\boldsymbol{\omega}}^{jO}_j \boldsymbol{N} \dot{\bar{\boldsymbol{u}}}^{jj}_{n_{el}} \end{bmatrix} \rho_p dV. \tag{43}$$

Finally, substitution of Eqs. (34), (37), (38), and (39) into the expression for the virtual work by inertia forces for the fluid (Eq. (31)) yields

$$\delta W_{in,f} = \begin{bmatrix} \delta \boldsymbol{r}^{OO}_j \\ \delta \boldsymbol{\pi}^{OO}_j \\ \delta \bar{\boldsymbol{u}}^{jj}_{n_{el}} \\ \delta s \end{bmatrix}^T \begin{bmatrix} \hat{\boldsymbol{R}}^O_j & \boldsymbol{0} \\ \boldsymbol{0} & 1 \end{bmatrix} \boldsymbol{\Upsilon}^T_{el} \left(\boldsymbol{M}^j_{f,el} \boldsymbol{\Upsilon}_{el} \begin{bmatrix} \hat{\boldsymbol{R}}^j_O & \boldsymbol{0} \\ \boldsymbol{0} & 1 \end{bmatrix} \begin{bmatrix} \ddot{\boldsymbol{r}}^{OO}_j \\ \dot{\boldsymbol{\omega}}^{OO}_j \\ \ddot{\bar{\boldsymbol{u}}}^{jj}_{n_{el}} \\ \ddot{s} \end{bmatrix} + \boldsymbol{D}^j_{f,el} \right) \tag{44}$$

with the element mass matrix of the fluid

$$\boldsymbol{M}^j_{f,el} = \int_V \begin{bmatrix} \boldsymbol{1} & (\tilde{\boldsymbol{r}}^{jj})^T & \boldsymbol{N} & \boldsymbol{N}' \\ \tilde{\boldsymbol{r}}^{jj} & \tilde{\boldsymbol{r}}^{jj}(\tilde{\boldsymbol{r}}^{jj})^T & \tilde{\boldsymbol{r}}^{jj}\boldsymbol{N} & \tilde{\boldsymbol{r}}^{jj}\boldsymbol{N}' \\ \boldsymbol{N}^T & \boldsymbol{N}^T(\tilde{\boldsymbol{r}}^{jj})^T & \boldsymbol{N}^T\boldsymbol{N} & \boldsymbol{N}^T\boldsymbol{N}' \\ (\boldsymbol{N}')^T & (\boldsymbol{N}')^T(\tilde{\boldsymbol{r}}^{jj})^T & (\boldsymbol{N}')^T\boldsymbol{N} & (\boldsymbol{N}')^T\boldsymbol{N}' \end{bmatrix} \rho_f dV, \tag{45}$$

the quadratic velocity terms for a fluid element

$$\boldsymbol{D}^j_{f,el} = \int_V \begin{bmatrix} \tilde{\boldsymbol{\omega}}^{jO}_j (\tilde{\boldsymbol{r}}^{jj})^T \boldsymbol{\omega}^{jO}_j + 2\tilde{\boldsymbol{\omega}}^{jO}_j \boldsymbol{N} \dot{\bar{\boldsymbol{u}}}^{jj}_{n_{el}} \\ \tilde{\boldsymbol{r}}^{jj} \tilde{\boldsymbol{\omega}}^{jO}_j (\tilde{\boldsymbol{r}}^{jj})^T \boldsymbol{\omega}^{jO}_j + 2\tilde{\boldsymbol{r}}^{jj} \tilde{\boldsymbol{\omega}}^{jO}_j \boldsymbol{N} \dot{\bar{\boldsymbol{u}}}^{jj}_{n_{el}} \\ \boldsymbol{N}^T \tilde{\boldsymbol{\omega}}^{jO}_j (\tilde{\boldsymbol{r}}^{jj})^T \boldsymbol{\omega}^{jO}_j + 2\boldsymbol{N}^T \tilde{\boldsymbol{\omega}}^{jO}_j \boldsymbol{N} \dot{\bar{\boldsymbol{u}}}^{jj}_{n_{el}} \\ (\boldsymbol{N}')^T \tilde{\boldsymbol{\omega}}^{jO}_j (\tilde{\boldsymbol{r}}^{jj})^T \boldsymbol{\omega}^{jO}_j + 2(\boldsymbol{N}')^T \tilde{\boldsymbol{\omega}}^{jO}_j \boldsymbol{N} \dot{\bar{\boldsymbol{u}}}^{jj}_{n_{el}} \\ + \{2\tilde{\boldsymbol{\omega}}^{jO}_j \boldsymbol{N}'(\bar{\boldsymbol{x}}^{jj}_{n_{el}} + \bar{\boldsymbol{u}}^{jj}_{n_{el}}) + 2\boldsymbol{N}' \dot{\bar{\boldsymbol{u}}}^{jj}_{n_{el}} + \boldsymbol{N}''(\bar{\boldsymbol{x}}^{jj}_{n_{el}} + \bar{\boldsymbol{u}}^{jj}_{n_{el}})\dot{s}\}\dot{s} \\ + \tilde{\boldsymbol{r}}^{jj}\{2\tilde{\boldsymbol{\omega}}^{jO}_j \boldsymbol{N}'(\bar{\boldsymbol{x}}^{jj}_{n_{el}} + \bar{\boldsymbol{u}}^{jj}_{n_{el}}) + 2\boldsymbol{N}' \dot{\bar{\boldsymbol{u}}}^{jj}_{n_{el}} + \boldsymbol{N}''(\bar{\boldsymbol{x}}^{jj}_{n_{el}} + \bar{\boldsymbol{u}}^{jj}_{n_{el}})\dot{s}\}\dot{s} \\ + \boldsymbol{N}^T\{2\tilde{\boldsymbol{\omega}}^{jO}_j \boldsymbol{N}'(\bar{\boldsymbol{x}}^{jj}_{n_{el}} + \bar{\boldsymbol{u}}^{jj}_{n_{el}}) + 2\boldsymbol{N}' \dot{\bar{\boldsymbol{u}}}^{jj}_{n_{el}} + \boldsymbol{N}''(\bar{\boldsymbol{x}}^{jj}_{n_{el}} + \bar{\boldsymbol{u}}^{jj}_{n_{el}})\dot{s}\}\dot{s} \\ + (\boldsymbol{N}')^T\{2\tilde{\boldsymbol{\omega}}^{jO}_j \boldsymbol{N}'(\bar{\boldsymbol{x}}^{jj}_{n_{el}} + \bar{\boldsymbol{u}}^{jj}_{n_{el}}) + 2\boldsymbol{N}' \dot{\bar{\boldsymbol{u}}}^{jj}_{n_{el}} + \boldsymbol{N}''(\bar{\boldsymbol{x}}^{jj}_{n_{el}} + \bar{\boldsymbol{u}}^{jj}_{n_{el}})\dot{s}\}\dot{s} \end{bmatrix} \rho_f dV, \tag{46}$$

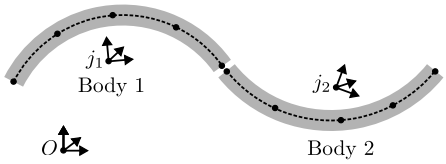

Fig. 2 A schematic illustration of a fluid-conveying pipe composed of two bodies, each consisting of four elements

and

$$\boldsymbol{\Upsilon}_{el} = \begin{bmatrix} \mathbf{1} & \mathbf{0} \\ \mathbf{0} & \tilde{\boldsymbol{x}}^{jj}_{n_{el}} + \tilde{\boldsymbol{u}}^{jj}_{n_{el}} \end{bmatrix}. \tag{47}$$

For an element with two nodes, $\boldsymbol{\Upsilon}_{el}$ is a matrix of dimensions 30×19.

5 Assembly on body level

A fluid-conveying pipe on system level consists of one or more fluid-conveying pipe bodies, and each body consists of one or multiple fluid-conveying pipe elements defined using the same floating frame. This is illustrated in Fig. 2 for a fluid-conveying pipe, which consists of two bodies, and where each body consists of four elements. In the previous sections the virtual work terms for one element of a body have been derived and resulted in expressions for the element mass matrix of the fluid and pipe, the quadratic velocity terms for an element of the fluid and pipe and the element stiffness matrix of the pipe. If the body consists of one element, then Eq. (24) can be used to obtain the equations of motion of the body. However, if the body consists of multiple elements, then assembly of the element level expressions for the components of the virtual work is required to obtain the equations of motion on body level. In this section, the equations of motion on body level are derived, followed by a discussion on model order reduction.

5.1 Equations of motion on body level

To obtain the virtual work components on body level, the virtual work components on element level must be assembled. For the pipe, the assembly is trivial and can be found in textbooks such as [27]. The assembled mass matrix, quadratic velocity terms, and stiffness matrix of the pipe on body level are denoted by $\boldsymbol{M}^j_p$, $\boldsymbol{D}^j_p$, and $\boldsymbol{K}^j_p$, respectively. As such, the virtual work by to elastic forces is written as

$$\delta W_{el,p} = (\delta \bar{\boldsymbol{u}}^{jj}_{n_b})^T \boldsymbol{K}^j_p \bar{\boldsymbol{u}}^{jj}_{n_b}, \tag{48}$$

and the virtual work inertia forces as

$$\delta W_{in,p} = \begin{bmatrix} \delta \boldsymbol{r}^{OO}_j \\ \delta \boldsymbol{\pi}^{OO}_j \\ \delta \bar{\boldsymbol{u}}^{jj}_{n_b} \end{bmatrix}^T \begin{bmatrix} \hat{\boldsymbol{R}}^O_j \end{bmatrix} \left(\boldsymbol{M}^j_p \begin{bmatrix} \hat{\boldsymbol{R}}^j_O \end{bmatrix} \begin{bmatrix} \ddot{\boldsymbol{r}}^{OO}_j \\ \dot{\boldsymbol{\omega}}^{OO}_j \\ \ddot{\bar{\boldsymbol{u}}}^{jj}_{n_b} \end{bmatrix} + \boldsymbol{D}^j_p \right). \tag{49}$$

where $\bar{\boldsymbol{u}}^{jj}_{n_b}$ is the vector of nodal displacements at all nodes of the body (n_b). For elements with two nodes, $\bar{\boldsymbol{u}}^{jj}_{n_b}$ is a vector of dimensions $(6N_{el}+6) \times 1$, with N_{el} denoting the number of elements of the body.

Assembling the virtual work by inertia forces for the fluid element shown in Eq. (44) to body level yields

$$\delta W_{in,f} = \begin{bmatrix} \delta \boldsymbol{r}_j^{OO} \\ \delta \boldsymbol{\pi}_j^{OO} \\ \delta \bar{\boldsymbol{u}}_{n_b}^{jj} \\ \delta s \end{bmatrix}^T \begin{bmatrix} \hat{\boldsymbol{R}}_j^O & \boldsymbol{0} \\ \boldsymbol{0} & 1 \end{bmatrix} \boldsymbol{\Upsilon}^T \left(\boldsymbol{M}_f^j \boldsymbol{\Upsilon} \begin{bmatrix} \hat{\boldsymbol{R}}_O^j & \boldsymbol{0} \\ \boldsymbol{0} & 1 \end{bmatrix} \begin{bmatrix} \ddot{\boldsymbol{r}}_j^{OO} \\ \dot{\boldsymbol{\omega}}_j^{OO} \\ \ddot{\bar{\boldsymbol{u}}}_{n_b}^{jj} \\ \ddot{s} \end{bmatrix} + \boldsymbol{D}_f^j \right) \tag{50}$$

with

$$\boldsymbol{\Upsilon} = \begin{bmatrix} \boldsymbol{1} & \boldsymbol{0} \\ \boldsymbol{0} & \bar{\boldsymbol{x}}_{n_b}^{jj} + \bar{\boldsymbol{u}}_{n_b}^{jj} \end{bmatrix}, \tag{51}$$

where $\bar{\boldsymbol{x}}_{n_b}^{jj}$ is the vector containing the local position and orientation of all nodes of the body in the undeformed configuration. For elements with two nodes, $\bar{\boldsymbol{x}}_{n_b}^{jj}$ is a vector of dimensions $(6N_{el}+6)\times 1$, and $\boldsymbol{\Upsilon}$ is a matrix of dimensions $(18+12N_{el})\times(13+6N_{el})$, and $\boldsymbol{M}_f^j$ and $\boldsymbol{D}_f^j$ denote the local mass matrix and local velocity-dependent terms for the fluid on body level and are obtained through assembly of the element matrices.

The equations of motion of the fluid-conveying pipe are obtained by substitution of Eqs. (26), (48), (49), and (50) into Eq. (24) and hold for all virtual displacements:

$$\begin{aligned} &\begin{bmatrix} \hat{\boldsymbol{R}}_j^O & \boldsymbol{0} \\ \boldsymbol{0} & 1 \end{bmatrix} \boldsymbol{\Upsilon}^T \left(\begin{bmatrix} \boldsymbol{M}_p^j & \boldsymbol{0} \\ \boldsymbol{0} & 0 \end{bmatrix} + \boldsymbol{M}_f^j \right) \boldsymbol{\Upsilon} \begin{bmatrix} \hat{\boldsymbol{R}}_O^j & \boldsymbol{0} \\ \boldsymbol{0} & 1 \end{bmatrix} \begin{bmatrix} \ddot{\boldsymbol{r}}_j^{OO} \\ \dot{\boldsymbol{\omega}}_j^{OO} \\ \ddot{\bar{\boldsymbol{u}}}_{n_b}^{jj} \\ \ddot{s} \end{bmatrix} \\ &\quad + \begin{bmatrix} \hat{\boldsymbol{R}}_j^O & \boldsymbol{0} \\ \boldsymbol{0} & 1 \end{bmatrix} \boldsymbol{\Upsilon}^T \left(\begin{bmatrix} \boldsymbol{D}_p^j \\ 0 \end{bmatrix} + \boldsymbol{D}_f^j \right) + \begin{bmatrix} \boldsymbol{0} \\ \boldsymbol{K}_p^j \\ 0 \end{bmatrix} \bar{\boldsymbol{u}}_{n_b}^{jj} = \begin{bmatrix} \boldsymbol{Q}^O \\ Q_s^O \end{bmatrix}. \end{aligned} \tag{52}$$

5.2 Model order reduction on body level

The degrees of freedom of the equations of motion shown in Eq. (52) are the six floating frame coordinates and elastic nodal displacements and the flow velocity along the centerline of the pipe. As the number of elements used to define a fluid-conveying pipe may be large, model order reduction techniques can be applied on the local elastic nodal displacements to achieve reduction of the computational cost of the simulation. Let the elastic nodal displacements $\bar{\boldsymbol{u}}_{n_b}^{jj}$ be approximated by a reduction basis $\boldsymbol{\Phi}$ so that

$$\bar{\boldsymbol{u}}_{n_b}^{jj} \approx \boldsymbol{\Phi}\boldsymbol{\eta}, \tag{53}$$

where $\boldsymbol{\eta}$ are the time-dependent elastic coordinates corresponding to $\boldsymbol{\Phi}$. As the local elastic nodal displacements are assumed to remain small with respect to the size of the body, many well-known techniques may be used to define the reduction basis, such as modal truncation [10] or component mode synthesis methods [11–13].

The reduction basis serves a secondary purpose. The system of equations as derived so far (Eq. (52)) is a singular system, as there is a redundancy between the floating frame coordinates and local elastic coordinates. As the position and orientation of the floating frame with respect to the deformed body have not been defined, a deformed body in the

global frame can be described by infinitely many combinations of choices for the floating frame and local elastic coordinates. By defining a reduction basis that cannot describe rigid-body motion, a nonsingular system of equations is obtained. Different methods to achieve this are discussed in [10] and [28], such as removing rigid body modes from the reduction basis through eigenvalue analysis or constraining the elastic deformation at the location of the floating frame to zero.

Substitution of Eq. (53) into the equations of motion of the fluid-conveying pipe shown in Eq. (52) allows us to write the reduced equations of motion as

$$\begin{bmatrix} \hat{\boldsymbol{R}}_j^O & \boldsymbol{0} \\ \boldsymbol{0} & 1 \end{bmatrix} \bar{\boldsymbol{\Upsilon}}^T \left(\begin{bmatrix} \boldsymbol{M}_p^j & \boldsymbol{0} \\ \boldsymbol{0} & 0 \end{bmatrix} + \boldsymbol{M}_f^j \right) \bar{\boldsymbol{\Upsilon}} \begin{bmatrix} \hat{\boldsymbol{R}}_O^j & \boldsymbol{0} \\ \boldsymbol{0} & 1 \end{bmatrix} \begin{bmatrix} \ddot{\boldsymbol{r}}_j^{OO} \\ \dot{\boldsymbol{\omega}}_j^{OO} \\ \ddot{\boldsymbol{\eta}} \\ \ddot{s} \end{bmatrix} + \begin{bmatrix} \hat{\boldsymbol{R}}_j^O & \boldsymbol{0} \\ \boldsymbol{0} & 1 \end{bmatrix} \bar{\boldsymbol{\Upsilon}}^T \left(\begin{bmatrix} \boldsymbol{D}_p^j \\ 0 \end{bmatrix} + \boldsymbol{D}_f^j \right) + \begin{bmatrix} \boldsymbol{0} \\ \boldsymbol{\Phi}^T \boldsymbol{K}_p^j \boldsymbol{\Phi} \\ 0 \end{bmatrix} \boldsymbol{\eta} = \begin{bmatrix} \begin{bmatrix} \boldsymbol{1} & \boldsymbol{0} \\ \boldsymbol{0} & \boldsymbol{\Phi}^T \end{bmatrix} \boldsymbol{Q}^O \\ Q_s^O \end{bmatrix}, \tag{54}$$

where $\bar{\boldsymbol{\Upsilon}}$ is a shorthand for the mode matrix

$$\bar{\boldsymbol{\Upsilon}} = \begin{bmatrix} \boldsymbol{1} & \boldsymbol{0} & \boldsymbol{0} \\ \boldsymbol{0} & \boldsymbol{\Phi} & \boldsymbol{0} \\ \boldsymbol{0} & \boldsymbol{0} & \bar{\boldsymbol{x}}_{n_b}^{jj} + \bar{\boldsymbol{u}}_{n_b}^{jj} \end{bmatrix} \tag{55}$$

of dimensions $(12 + N_m + 6N_{el}) \times (7 + N_m)$ with N_m denoting the number of modes in the reduction basis.

6 Constrained equations of motion

To formulate the constrained equations of motion of the fluid-conveying pipe, the unconstrained equations of motion shown in Eq. (54) must be formulated for all bodies in the system and combined with kinematic constraints. As the kinematic constraints imposed on each body must be expressed as functions of the global floating frame coordinates and local elastic coordinates, the constraint equations are nonlinear. Therefore Lagrange multipliers are used to formulate the constrained equations of motion [29]. The holonomic kinematic constraint equations can be written as

$$\boldsymbol{C} = \boldsymbol{0}, \tag{56}$$

where the constraints $\boldsymbol{C}$ are functions of the global floating frame coordinates and local elastic coordinates. The second derivative of the constraint relations with respect to time yields the acceleration equation

$$\boldsymbol{C}_{\boldsymbol{q}} \ddot{\boldsymbol{q}} = -[\boldsymbol{C}_{\boldsymbol{q}} \dot{\boldsymbol{q}}]_{\boldsymbol{q}} \dot{\boldsymbol{q}} - 2\dot{\boldsymbol{C}}_{\boldsymbol{q}} \dot{\boldsymbol{q}} - \ddot{\boldsymbol{C}}, \tag{57}$$

where $\dot{\boldsymbol{q}}$ and $\ddot{\boldsymbol{q}}$ are the vectors of generalized velocities and generalized accelerations, respectively, such that

$$\dot{\boldsymbol{q}} = \begin{bmatrix} \dot{\boldsymbol{r}}_j^{OO} \\ \boldsymbol{\omega}_j^{OO} \\ \dot{\boldsymbol{\eta}} \end{bmatrix} \quad \text{and} \quad \ddot{\boldsymbol{q}} = \begin{bmatrix} \ddot{\boldsymbol{r}}_j^{OO} \\ \dot{\boldsymbol{\omega}}_j^{OO} \\ \ddot{\boldsymbol{\eta}} \end{bmatrix} \tag{58}$$

if the system is composed of one body. If the system is composed of multiple bodies, then $\dot{\boldsymbol{q}}$ and $\ddot{\boldsymbol{q}}$ contain the generalized coordinates of each body. Furthermore, $\boldsymbol{C}_{\boldsymbol{q}}$ is the Jacobian of the constraints, and $[\boldsymbol{C}_{\boldsymbol{q}}\dot{\boldsymbol{q}}]_{\boldsymbol{q}}$ is the Jacobian of the product between the brackets. Using the Lagrange multipliers $\boldsymbol{\lambda}$ to combine the acceleration equation shown in Eq. (57) with the equations of motion shown in Eq. (54) allows us to formulate the constrained equations of motion in augmented form for a fluid-conveying pipe as

$$\begin{bmatrix} \begin{bmatrix} \hat{\boldsymbol{R}}_j^O & \boldsymbol{0} \\ \boldsymbol{0} & 1 \end{bmatrix} \bar{\boldsymbol{\Upsilon}}^T \left(\begin{bmatrix} \boldsymbol{M}_p^j & \boldsymbol{0} \\ \boldsymbol{0} & 0 \end{bmatrix} + \boldsymbol{M}_f^j \right) \bar{\boldsymbol{\Upsilon}} \begin{bmatrix} \hat{\boldsymbol{R}}_O^j & \boldsymbol{0} \\ \boldsymbol{0} & 1 \end{bmatrix} & \boldsymbol{C}_{\boldsymbol{q}}^T \\ \boldsymbol{C}_{\boldsymbol{q}} & \boldsymbol{0} \end{bmatrix} \begin{bmatrix} \begin{bmatrix} \ddot{\boldsymbol{q}} \\ \ddot{s} \end{bmatrix} \\ \boldsymbol{\lambda} \end{bmatrix}$$
$$= \begin{bmatrix} \begin{bmatrix} \begin{bmatrix} \boldsymbol{1} & \boldsymbol{0} \\ \boldsymbol{0} & \boldsymbol{\Phi}^T \end{bmatrix} \boldsymbol{Q}^O \\ Q_s^O \end{bmatrix} - \begin{bmatrix} \hat{\boldsymbol{R}}_j^O & \boldsymbol{0} \\ \boldsymbol{0} & 1 \end{bmatrix} \bar{\boldsymbol{\Upsilon}}^T \left(\begin{bmatrix} \boldsymbol{D}_p^j \\ 0 \end{bmatrix} + \boldsymbol{D}_f^j \right) - \begin{bmatrix} \boldsymbol{0} \\ \boldsymbol{\Phi}^T \boldsymbol{K}_p^j \boldsymbol{\Phi} \\ 0 \end{bmatrix} \boldsymbol{\eta} \\ -[\boldsymbol{C}_{\boldsymbol{q}}\dot{\boldsymbol{q}}]_{\boldsymbol{q}}\dot{\boldsymbol{q}} - 2\dot{\boldsymbol{C}}_{\boldsymbol{q}}\dot{\boldsymbol{q}} - \ddot{\boldsymbol{C}} \end{bmatrix} \tag{59}$$

for a system composed of one body. If the system consists of multiple bodies, then Eq. (59) must be assembled for each body in the system. Equation (59) can be used to simulate a system consisting solely of fluid-conveying pipe elements but can also be combined with other elements through kinematic constraints to simulate a mechanical system that contains fluid-conveying pipes.

In many applications, the velocity and acceleration of the fluid are controlled variables and can therefore be assumed as known in the context of the current analysis [6]. For a prescribed velocity and acceleration of the fluid, the equation corresponding to the force responsible for the axial movement of the fluid Q_s^O in Eq. (59) can be omitted.

7 Simplification for efficient incorporation in multibody software

Implementing the fluid-conveying pipe elements as developed so far requires evaluation of the volume integrals that comprise the element mass matrices and element quadratic velocity terms [27]. Most implementations of the FFRF avoid computation of these integrals. For solid elements, this is typically done by approximating the volume integrals using the (lumped) finite element mass matrix. However, as the fluid-conveying pipe elements contain volume integrals that are not present for solid elements, we must consider how the fluid-conveying pipe elements can be implemented in practice. Therefore we propose a simplification of the derived element mass matrix and quadratic velocity terms.

Since the volume integrals unique to the fluid-conveying pipe elements require information about the derivatives of the shape functions, the (lumped) finite element mass matrix alone is not sufficient to approximate them. Therefore, for the fluid-conveying pipe elements developed in this work to be incorporated within multibody software packages, knowledge of the derivatives of the shape functions must either be imported into the software package or hardcoded within it. Given that the shapes of fluid-conveying pipes can vary significantly, a large variety of shape functions is required. To minimize the hardcoding involved with the implementation of the developed elements, we propose a further simplification. Any slender pipe shape can be approximated by preimposing deformation upon the model of a straight pipe. The preimposed deformation must be determined a priori, and a stiffness term must be added to ensure that the initial state corresponds with the desired stress state. The proviso for this approach is that the deformation within each body remains small. Therefore a pipe shape with large curvature must be modeled using multiple bodies.

7.1 Simplification on element level

Consider one fluid-conveying pipe element. The rigid body modes of the undeformed element ($\boldsymbol{\Psi}_{0,el}$) can be written as

$$\boldsymbol{\Psi}_{0,el} = \begin{bmatrix} \mathbf{1} & (\tilde{\boldsymbol{x}}_1^{jj})^T \\ \mathbf{0} & \mathbf{1} \\ \mathbf{1} & (\tilde{\boldsymbol{x}}_2^{jj})^T \\ \mathbf{0} & \mathbf{1} \end{bmatrix} \quad \text{with} \quad \boldsymbol{\Psi}_{r0,el} = \begin{bmatrix} (\tilde{\boldsymbol{x}}_1^{jj})^T \\ \mathbf{1} \\ (\tilde{\boldsymbol{x}}_2^{jj})^T \\ \mathbf{1} \end{bmatrix}, \tag{60}$$

where the subscripts 1 and 2 denote the nodes of the element. Each column of $\begin{bmatrix} \mathbf{1} & \mathbf{0} & \mathbf{1} & \mathbf{0} \end{bmatrix}^T$ represents a rigid translation of the element, and each column of $\begin{bmatrix} \tilde{\boldsymbol{x}}_1^{jj} & \mathbf{1} & \tilde{\boldsymbol{x}}_2^{jj} & \mathbf{1} \end{bmatrix}^T$ represents rigid rotation of the undeformed element about the floating frame ($\boldsymbol{\Psi}_{r0,el}$). Since no stresses are introduced due to rigid body motion and the partition of unity must be satisfied, we have that

$$\mathbf{1} = \boldsymbol{N}(\boldsymbol{x}^{jj}) \begin{bmatrix} \mathbf{1} \\ \mathbf{0} \\ \mathbf{1} \\ \mathbf{0} \end{bmatrix} \quad \text{and} \quad (\tilde{\boldsymbol{x}}^{jj})^T = \boldsymbol{N}(\boldsymbol{x}^{jj}) \begin{bmatrix} (\tilde{\boldsymbol{x}}_1^{jj})^T \\ \mathbf{1} \\ (\tilde{\boldsymbol{x}}_2^{jj})^T \\ \mathbf{1} \end{bmatrix}. \tag{61}$$

Although the expression for $\tilde{\boldsymbol{x}}^{jj}$ shown in Eq. (61) is exact for any material point on the undeformed element, its equivalent for a deformed element is not:

$$(\tilde{\boldsymbol{r}}^{jj})^T \approx \boldsymbol{N}(\boldsymbol{x}^{jj}) \begin{bmatrix} (\tilde{\boldsymbol{r}}_1^{jj})^T \\ \mathbf{1} \\ (\tilde{\boldsymbol{r}}_2^{jj})^T \\ \mathbf{1} \end{bmatrix}. \tag{62}$$

Equation (62) is an approximation when evaluated at an internal material point. However, it is exact at the nodes of the element, because the shape functions simplify to a matrix of zeros and an identity matrix of dimensions 3×3 corresponding to the translational degrees of freedom of the node in question. The assumptions of small elastic deformations allow us to approximate

$$\tilde{\boldsymbol{r}}^{jj} \approx \tilde{\boldsymbol{x}}^{jj}. \tag{63}$$

Therefore, by substituting Eqs. (60), (61), and (63) into the element mass matrices of the pipe and fluid, an approximation for the mass matrices can be obtained for which the volume integrals are less tedious to implement and remain constant throughout the simulation. Note that due to the application of Eq. (63), the mass matrix of the undeformed configuration is used to approximate the mass matrix of the deformed configuration. Alternatively, Eq. (62) could be implemented.

Substitution of Eqs. (60), (61), and (63) into the element mass matrix of the pipe shown in Eq. (42) yields

$$\boldsymbol{M}_{p,el}^{j} \approx \begin{bmatrix} \boldsymbol{\Psi}_{0,el}^T \\ \mathbf{1} \end{bmatrix} \int_V \boldsymbol{N}^T \boldsymbol{N} \rho_p dV \begin{bmatrix} \boldsymbol{\Psi}_{0,el} & \mathbf{1} \end{bmatrix}, \tag{64}$$

from which we can recognize $\int_V \boldsymbol{N}^T \boldsymbol{N} \rho_p dV$ as the finite element mass matrix. Substitution of Eqs. (60), (61), and (63) into the element mass matrix of the fluid shown in Eq. (45) yields

$$\begin{aligned}\boldsymbol{\Upsilon}_{el}^T \boldsymbol{M}_{f,el}^j \boldsymbol{\Upsilon}_{el} \approx & \begin{bmatrix} \begin{bmatrix} \boldsymbol{\Psi}_{0,el}^T \\ \mathbf{1} \end{bmatrix} & \mathbf{0} \\ \mathbf{0} & (\bar{\boldsymbol{x}}_{n_{el}}^{jj} + \bar{\boldsymbol{u}}_{n_{el}}^{jj})^T \end{bmatrix} \\ & \times \int_V \begin{bmatrix} \boldsymbol{N}^T \boldsymbol{N} & \boldsymbol{N}^T \boldsymbol{N}' \\ (\boldsymbol{N}')^T \boldsymbol{N} & (\boldsymbol{N}')^T \boldsymbol{N}' \end{bmatrix} \rho_p dV \begin{bmatrix} \begin{bmatrix} \boldsymbol{\Psi}_{0,el} & \mathbf{1} \\ \mathbf{0} \end{bmatrix} & \mathbf{0} \\ & \bar{\boldsymbol{x}}_{n_{el}}^{jj} + \bar{\boldsymbol{u}}_{n_{el}}^{jj} \end{bmatrix}. \end{aligned} \tag{65}$$

Similarly, the quadratic velocity terms of a pipe element shown in Eq. (43) can, by substitution of Eqs. (61), (60), and (63), be written as

$$\boldsymbol{D}_{p,el}^j \approx \begin{bmatrix} \boldsymbol{\Psi}_{0,el}^T \\ \mathbf{1} \end{bmatrix} \int_V \boldsymbol{N}^T \tilde{\boldsymbol{\omega}}_j^{jO} \boldsymbol{N} \rho_p dV \left(\boldsymbol{\Psi}_{r0,el} \tilde{\boldsymbol{\omega}}_j^{jO} + 2\dot{\bar{\boldsymbol{u}}}_{n_{el}}^{jj} \right) \tag{66}$$

with

$$\boldsymbol{\Psi}_{r0,el} \tilde{\boldsymbol{\omega}}_j^{jO} + 2\dot{\bar{\boldsymbol{u}}}_{n_{el}}^{jj} = \begin{bmatrix} (\tilde{\boldsymbol{x}}_1^{jj})^T \boldsymbol{\omega}_j^{jO} + 2\dot{\boldsymbol{r}}_1^{jj} \\ \boldsymbol{\omega}_j^{jO} + 2\boldsymbol{\omega}_1^{jj} \\ (\tilde{\boldsymbol{x}}_2^{jj})^T \boldsymbol{\omega}_j^{jO} + 2\dot{\boldsymbol{r}}_2^{jj} \\ \boldsymbol{\omega}_j^{jO} + 2\boldsymbol{\omega}_2^{jj} \end{bmatrix}. \tag{67}$$

Finally, the quadratic velocity terms of the fluid element (Eq. (46)) can be approximated as

$$\begin{aligned}\boldsymbol{\Upsilon}_{el}^T \boldsymbol{D}_{f,el}^j \approx & \begin{bmatrix} \begin{bmatrix} \boldsymbol{\Psi}_{0,el}^T \\ \mathbf{1} \end{bmatrix} & \mathbf{0} \\ \mathbf{0} & (\bar{\boldsymbol{x}}_{n_{el}}^{jj} + \bar{\boldsymbol{u}}_{n_{el}}^{jj})^T \end{bmatrix} \\ & \times \int_V \begin{bmatrix} \boldsymbol{N}^T \tilde{\boldsymbol{\omega}}_j^{jO} \boldsymbol{N} & \boldsymbol{N}^T \tilde{\boldsymbol{\omega}}_j^{jO} \boldsymbol{N}' & \boldsymbol{N}^T \boldsymbol{N}' & \boldsymbol{N}^T \boldsymbol{N}'' \\ (\boldsymbol{N}')^T \tilde{\boldsymbol{\omega}}_j^{jO} \boldsymbol{N} & (\boldsymbol{N}')^T \tilde{\boldsymbol{\omega}}_j^{jO} \boldsymbol{N}' & (\boldsymbol{N}')^T \boldsymbol{N}' & (\boldsymbol{N}')^T \boldsymbol{N}'' \end{bmatrix} \rho_p dV \\ & \begin{bmatrix} \boldsymbol{\Psi}_{r0,el} \tilde{\boldsymbol{\omega}}_j^{jO} + 2\dot{\bar{\boldsymbol{u}}}_{n_{el}}^{jj} \\ 2(\bar{\boldsymbol{x}}_{n_{el}}^{jj} + \bar{\boldsymbol{u}}_{n_{el}}^{jj})\dot{s} \\ 2\dot{\bar{\boldsymbol{u}}}_{n_{el}}^{jj} \dot{s} \\ (\bar{\boldsymbol{x}}_{n_{el}}^{jj} + \bar{\boldsymbol{u}}_{n_{el}}^{jj})\dot{s}^2 \end{bmatrix}. \end{aligned} \tag{68}$$

Note that by utilization of

$$\tilde{\boldsymbol{\omega}}_j^{jO} = \tilde{\boldsymbol{n}}_x (\boldsymbol{\omega}_j^{jO})_x + \tilde{\boldsymbol{n}}_y (\boldsymbol{\omega}_j^{jO})_y + \tilde{\boldsymbol{n}}_z (\boldsymbol{\omega}_j^{jO})_z \tag{69}$$

all volume integrals that comprise the element mass matrices and quadratic velocity terms are constant over time.

7.2 Assembly and reduction

Model order reduction can be implemented to reduce the number degrees of freedom in the system. Note that by selecting a reduction basis that cannot describe rigid-body motion the singularity caused by the redundancy between the floating frame coordinates and local elastic coordinates is removed from the system of equations. A detailed explanation can be

found in Sect. 5.2, as the same method is applied to remove the singularity for the nonsimplified system of equations. The assembly to body level and the reduction of the equations of motion are performed according to the procedure described in Sect. 5 and therefore are not repeated in detail here.

The simplified mass matrix and quadratic velocity terms of the pipe on body level are denoted as $\hat{\boldsymbol{M}}_p^j$ and $\hat{\boldsymbol{D}}_p^j$, respectively. For the fluid, the simplified mass matrix and quadratic velocity terms on body level are denoted as $\hat{\boldsymbol{M}}_f^j$ and $\hat{\boldsymbol{D}}_f^j$. As such, the simplified constrained equations of motion for a prescribed velocity and acceleration of the fluid can be written as

$$\begin{aligned}
&\begin{bmatrix} \begin{bmatrix} \hat{\boldsymbol{R}}_j^O & \boldsymbol{0} \end{bmatrix} \hat{\boldsymbol{\Upsilon}}^T \left(\begin{bmatrix} \hat{\boldsymbol{M}}_p^j & \boldsymbol{0} \\ \boldsymbol{0} & 0 \end{bmatrix} + \hat{\boldsymbol{M}}_f^j \right) \hat{\boldsymbol{\Upsilon}} \begin{bmatrix} \hat{\boldsymbol{R}}_O^j & \boldsymbol{C}_{\boldsymbol{q}}^T \\ \boldsymbol{0} & \boldsymbol{0} \end{bmatrix} \begin{bmatrix} \ddot{\boldsymbol{q}} \\ \boldsymbol{\lambda} \end{bmatrix} \\
&\quad = \begin{bmatrix} \begin{bmatrix} \boldsymbol{1} & \boldsymbol{0} \\ \boldsymbol{0} & \boldsymbol{\Phi}^T \end{bmatrix} \boldsymbol{Q}^O - \begin{bmatrix} \hat{\boldsymbol{R}}_j^O & \boldsymbol{0} \end{bmatrix} \hat{\boldsymbol{\Upsilon}}^T \left(\hat{\boldsymbol{M}}_f^j \hat{\boldsymbol{\Upsilon}} \begin{bmatrix} \boldsymbol{0} \\ 1 \end{bmatrix} \ddot{s} + \begin{bmatrix} \hat{\boldsymbol{D}}_p^j \\ 0 \end{bmatrix} + \hat{\boldsymbol{D}}_f^j \right) - \begin{bmatrix} \boldsymbol{0} \\ \boldsymbol{\Phi}^T \boldsymbol{K}_p^j \boldsymbol{\Phi} \end{bmatrix} \boldsymbol{\eta} + \begin{bmatrix} \boldsymbol{0} \\ \boldsymbol{\Phi}^T \boldsymbol{K}_p^j \boldsymbol{\Phi} \end{bmatrix} \boldsymbol{\eta}_0 \\ -[\boldsymbol{C}_{\boldsymbol{q}} \dot{\boldsymbol{q}}]_{\boldsymbol{q}} \dot{\boldsymbol{q}} - 2\dot{\boldsymbol{C}}_{\boldsymbol{q}} \dot{\boldsymbol{q}} - \ddot{\boldsymbol{C}} \end{bmatrix},
\end{aligned} \tag{70}$$

where the mode matrix $\hat{\boldsymbol{\Upsilon}}$ is defined as

$$\hat{\boldsymbol{\Upsilon}} = \begin{bmatrix} \begin{bmatrix} \boldsymbol{\Psi}_0 & \boldsymbol{\Phi} \end{bmatrix} & \boldsymbol{0} \\ \boldsymbol{0} & \bar{\boldsymbol{x}}_{n_b}^{jj} + \bar{\boldsymbol{u}}_{n_b}^{jj} \end{bmatrix}, \tag{71}$$

and $\boldsymbol{\Psi}_0$ are the rigid modes of the undeformed body. The term $\boldsymbol{\Phi}^T \boldsymbol{K}_p^j \boldsymbol{\eta}_0$ is incorporated to ensure that the initial configuration corresponds to the desired stress state.

Implementation of the simplified constrained equations of motion in multibody software while minimizing the afford required on the side of the user may be as follows. Firstly, the centerline of the pipe must be created (using a CAD package) and imported into the multibody software. Secondly, the user must define the material properties and geometric properties of the fluid-conveying pipe, including the number of bodies with which to perform the simulation. Thirdly, an algorithm must be implemented that is able to partition the imported centerline into the defined number of bodies so that the curvature (the preimposed deformation) within the bodies is minimized. Finally, the compensation of the stiffness that follows from the preimposed deformation must be incorporated into the simulation.

8 Validation

To validate the method described in this work, we consider two example problems: a cantilevered straight pipe and a semicircular pipe, which is allowed to rotate about the out of plane axis. The results for both problems modeled with the simplified approach will be compared to results obtained using the established multibody software Spacar, which is based on finite elements [24]. A description of the fluid-conveying pipe elements implemented within the Spacar package can be found in [6]. To show that the developed fluid-conveying pipe elements can be integrated in a mechanical system, a simplified concrete 3D printing system is modeled as well.

The Craig–Bampton modes [11] are used as a reduction basis in each validation problem. To this end, the left- and rightmost nodes are defined as the boundary nodes of the body. Both the boundary and internal modes are calculated while constraining the deformation at the center node to zero. As such, the reduction basis cannot describe a rigid-body motion.

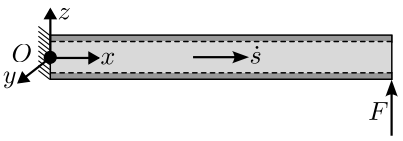

Fig. 3 A schematic illustration of the cantilevered straight pipe

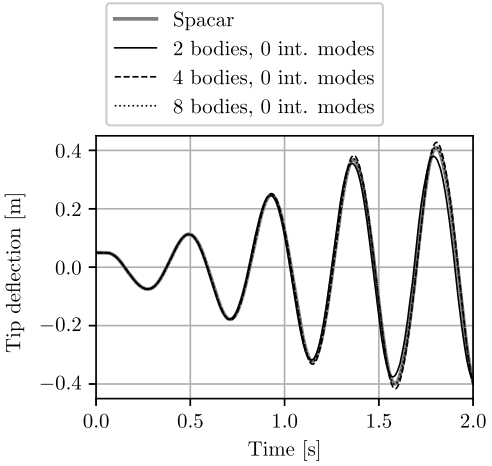

Fig. 4 The deflection of the free end of the pipe modeled with multiple bodies and zero internal modes

8.1 Straight pipe

Consider the cantilevered straight pipe illustrated in Fig. 3. The left end of the pipe is fixed and coincides with the global frame O. The pipe has a length of 1 m, an inner diameter of 50.46 mm, and an outer diameter of 61.97 mm. The density of the pipe is 7870 kg/m^3, and it has Young's modulus of 24.64 MPa and shear modulus of 9.48 MPa. The fluid has a density of 1000 kg/m^3 and flows with constant velocity through the pipe. A force F of 1.5 N is applied along the z-axis at the right end of the pipe. The selected parameters are based on the straight pipe problem shown in [6].

In the initial configuration, the pipe is at rest in the static equilibrium configuration corresponding to the applied force and a fluid velocity $\dot{s}$ of 0 m/s. The flow velocity is increased to 15 m/s while the applied force remains constant. The deflection of the right end of the pipe due to the fluid flow is shown in Fig. 4. The grey line in the figure shows the result obtained using Spacar [6, 24] for a pipe modeled with eight elements. The results obtained with the floating frame approach for a pipe modeled with two, four, and eight bodies are shown in black. Each body is comprised of 20 elements, and the reduction basis consists of the Craig–Bampton boundary modes [11]. As such, each body represents 18 degrees of freedom. Note that the number of (elastic) degrees of freedom in the Spacar model with eight elements equals the number of (elastic) degrees of freedom in the floating frame simulation with eight bodies. Accordingly, the result obtained using eight bodies closely resembles the Spacar result, whereas using fewer bodies causes differences in amplitude and frequency.

Representing the pipe with one body yields poor results, regardless of the number of internal modes included in the reduction basis in addition to the boundary modes. Figure 5 shows the deflection results for a simulation using one body and 0 or 20 internal modes. Refining the simulation with two bodies by using 20 internal modes does show improvement of the result, as presented in Fig. 5 as well.

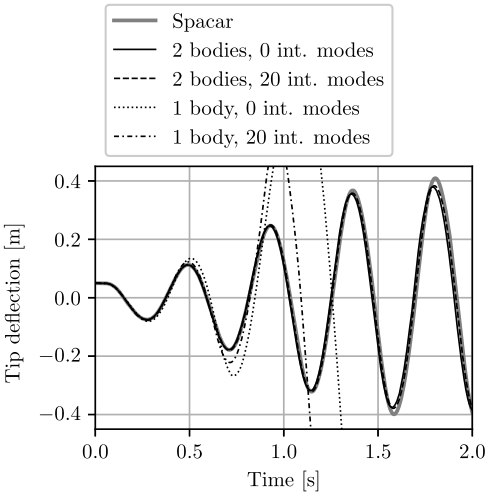

Fig. 5 The deflection of the free end of the pipe modeled with a limited number of bodies but including internal modes

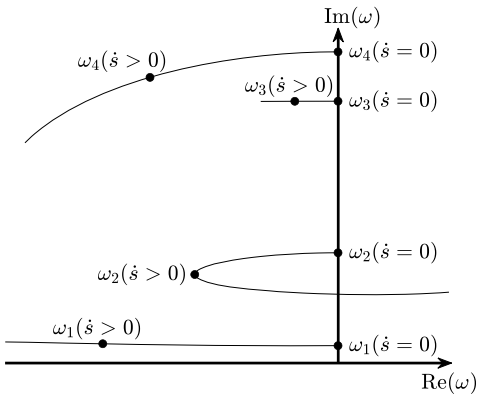

Fig. 6 An illustration of the development of the first four eigenvalues ω for increasing flow velocity $\dot{s}$. Note that the eigenvalues develop beyond what is shown in the figure

An analysis of the eigenvalues of the linearized system of equations allows us to identify the critical flow speed at which the cantilevered pipe becomes unstable, also known as the garden hose problem [1]. The eigenvalues of the constrained equations of motion can be determined by writing the system in embedded form, in this case expressed in terms of the modal coordinates, linearizing this system in its undeformed state and transforming it to state space form. As the flow speed is considered an input variable, the coupling term between the flow speed ($\dot{s}$) and the velocity of the configuration ($\dot{\boldsymbol{x}} + \dot{\boldsymbol{u}}$) as well as the square of the flow speed ($\dot{s}^2$) remain in the linearized system of equations, resulting in complex eigenvalues. The development of the first four eigenvalues ω for increasing flow rate is illustrated in Fig. 6. Note that only the positive imaginary axis is shown, although the complex conjugates of the eigenvalues exist as well. Hoph bifurcation [1] occurs when the second eigenfrequency crosses the imaginary axis. As at this flow velocity the second eigenfrequency obtains a positive real value, indicating an unstable system, the flow velocity corresponding to this transition is the critical flow speed and can be found by implementing a search algorithm that finds the flow speed corresponding to the crossing of the imaginary axis in Fig. 6.

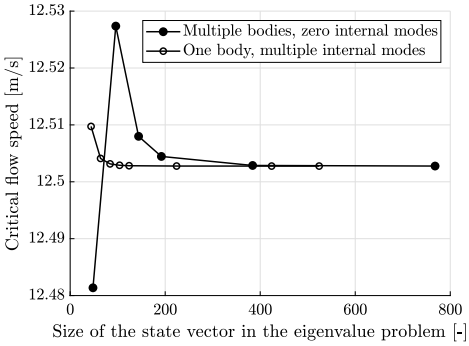

Fig. 7 The critical flow speed obtained for pipes modeled with a varying number of bodies and internal modes. The size of the state vector reflects the number of degrees of freedom in the model

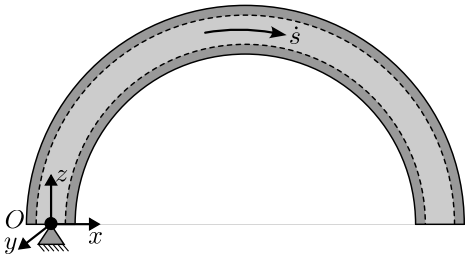

Fig. 8 A schematic illustration of the semicircular pipe

Figure 7 shows the critical flow speed found if the pipe is modeled with a different number of bodies and internal modes with respect to the size of the state vector used to describe the eigenvalue problem. The size of this state vector equals twice the sum of the number of static and internal Craig–Bampton modes multiplied by the number of bodies. The two graphs in the figure represent the critical flow velocity in case the number of bodies is refined but no internal modes are included (filled markers) and the critical flow velocity in case one body is used but the number of internal modes is refined (unfilled markers). Each body is modeled using 51 nodes. Although refining the number of bodies and the number of internal modes both converge to the same critical flow speed, refining the number of internal modes converges faster with respect to the size of the eigenvalue problem. However, as shown in the transient results, representing the pipe with one body is not sufficient if the system is nonlinear. The critical flow speed for a pipe modeled with 2, 4, 8, 16, and 32 bodies and no internal modes is equivalent to the critical flow speeds for the Spacar model with 2, 4, 8, 16, and 32 elements, as reported in [6], with five decimals precision.

8.2 Curved pipe

Consider the semicircular pipe shown in Fig. 8. The base of the pipe coincides with the global frame O and is fixed to the real world so that only the rotation about the y-axis remains unconstrained. The pipe has an inner and outer diameters of 35.68 and 36.80 mm, respectively. The radius of the circular shape of the pipe is 0.5 m. The pipe has a density of 7870 kg/m^3 and Poisson's ratio of 0.3. The density of the fluid is 1000 kg/m^3, and the flow velocity is 10 m/s. The pipe will be modeled using three different Young's moduli: 95.85, 9.585, and 0.9585 GPa. Young's modulus will influence the rotational velocity of the pipe induced by the flow, as the deformed shape of the pipe is dependent on Young's modulus. The selected parameters are based on the cantilevered pipe problem shown in [6].

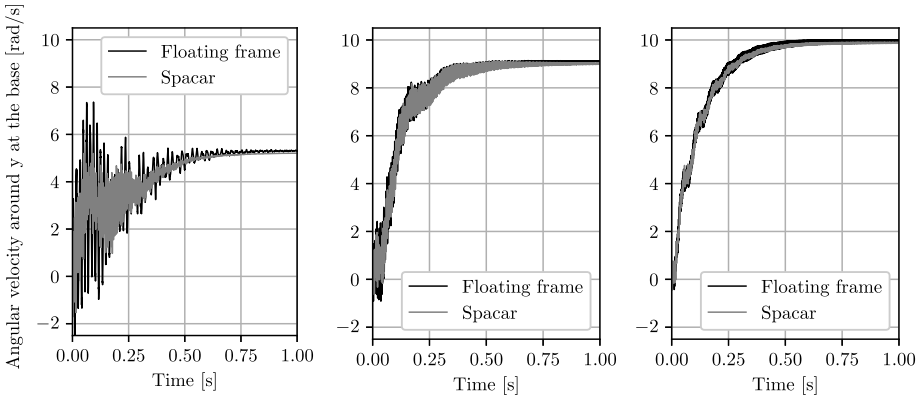

Fig. 9 The angular velocity about the y-axis at the base of the pipe for different Young's moduli. Left: $E = 0.9585$ GPa. Middle: $E = 9.585$ GPa. Right: $E = 95.85$ GPa

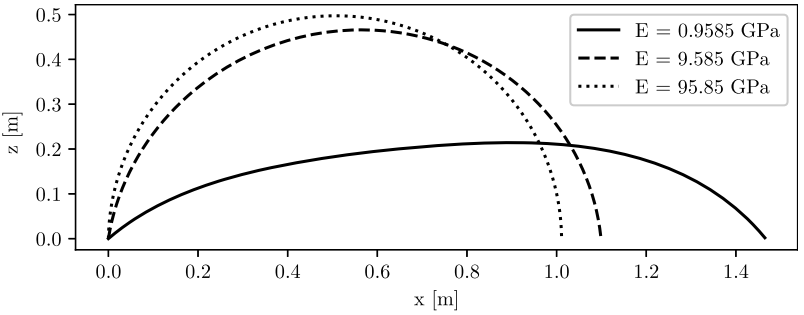

Fig. 10 The deformation of the pipe at the last time step of the simulations for different Young's moduli

The semicircular pipe is modeled using the interpolation functions of a straight beam. To obtain the circular shape, elastic deformation is preimposed, and a stiffness term is added to the equations of motion, which ensures that the semicircular shape corresponds to a stress-free state. Special care must be taken to ensure that no jumps in position and orientation occur between consecutive bodies. The pipe is modeled using eight bodies to comply with the assumption of small deformations. Each body is comprised of 20 elements. The reduction basis consists of Craig–Bampton boundary modes [11].

The angular velocity about the y-axis at the base of the pipe is shown for three Young's moduli in Fig. 9. The black lines represent the results obtained with the floating frame approach (no internal modes have been included), and the grey lines represent the results obtained with Spacar in case the pipe is modeled with eight elements. The angular velocity changes with different Young's moduli as the flow induced deformation of the pipe changes with Young's modulus. To illustrate this, the deformation of the pipes at the last time step of the simulations is shown in Fig. 10. The final angular velocity for both the Spacar and floating frame approach are listed in Table 1. The high frequent oscillations in angular velocity are the result of elongation of the pipe, as these oscillations are not present when simulating pipes thath cannot elongate, and differ between the two modeling approaches. The difference is largely due to small differences in the initial configuration between the

Table 1 The final angular velocity around the y-axis at the base of the pipe, obtained with the floating frame approach and Spacar for different Young's moduli

Young's modulus	Final angular velocity	
	Floating frame	Spacar
$E = 0.9585$ GPa	5.320 rad/s	5.218 rad/s
$E = 9.585$ GPa	9.117 rad/s	9.010 rad/s
$E = 95.85$ GPa	9.954 rad/s	9.882 rad/s

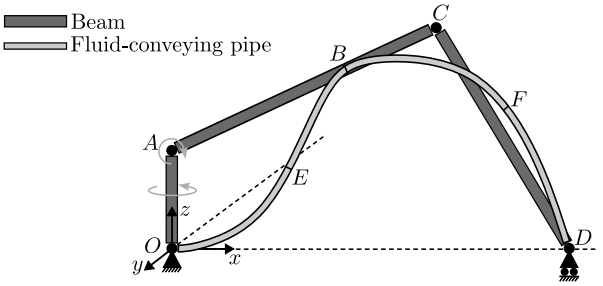

Fig. 11 A schematic illustration of the concrete printer

two approaches. The closer the initial shape to semicircular, the faster the convergence of the final angular velocity.

8.3 Cement-based concrete printer

To illustrate the integration of the developed fluid-conveying pipe elements within a multibody system, consider the model of a concrete printer shown in Fig. 11. Note that the model does not represent a realistic concrete printing system and the simulation results will not be validated against alternative software, as this example exclusively aims to demonstrate the applicability of the developed elements within the broader context of a multibody system. A robot arm consisting of the four bodies OA, AB, BC, and CD modeled as beams is used to position the nozzle for depositioning of concrete. The nozzle is attached to point D. At points O, A, and C the bodies are connected through hinge joints. As such, body OA can only rotate about the z-axis, whereas the joints at A and C only allow for rotation in the plane described by the connected bodies. Point D is connected to a roller that constraints the movement in the global z-axis. The bodies OA, AB, BC, and CD are comprised of 4, 10, 4, and 14 elements. The concrete-conveying pipe is modeled by four bodies as well: OE, EB, BF, and FD. Each is comprised of four elements. Each body is rigidly attached to the next. At point O, the pipe is constrained so that only the rotation about the global z-axis is free. At points B and D the pipe is attached to the robot arm while leaving the orientation of the pipe at these points unconstrained.

The length of the bodies OA, AB, BC, and CD of the robot arm are 0.15, 0.30, 0.15, and 0.40 m, respectively. Each of these bodies has a diameter of 4 cm, a density of 7870 kg/m^3, a Young's modulus of 200 GPa, and a shear modulus of 77 GPa. The bodies OE, EB, BF, and FD that form the pipe have the lengths 0.20, 0.20, 0.28, and 0.28 m, respectively. The outer diameter of the pipe is 4 cm, and the inner diameter is 3.5 cm. The pipe has a density of 1330 kg/m^3, a Young's modulus of 3.4 GPa, and a shear modulus of 1.2 GPa. These parameters are based on the properties of polyethylene terephthalate (PET). The density of the cement-based concrete flowing through the pipe is 2400 kg/m^3.

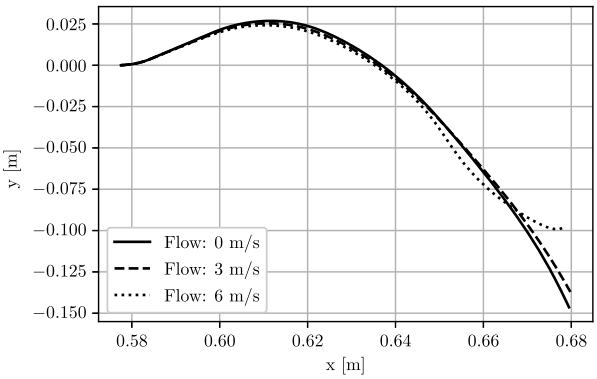

Fig. 12 The trajectories of point D in the xy-plane during 0.34 seconds in cases where flows of 0,3, and 6 m/s are modeled

When printing, the nozzle at point D must move smoothly along the desired trajectory in the xy-plane, while the concrete flow out of the nozzle is sufficiently high to create a concrete layer with the desired dimensions without tearing. However, as the density of the concrete is relatively high, a large flow speed of concrete might influence the trajectory of the nozzle and must be taken into account when determining the driving moments. This example illustrates this effect. In the initial configuration the system is at rest while a moment of -5000 Nm is applied at point A. The configuration of the pipe due to gravity is determined in a static analysis. The printing process is simulated by moving the robot arm in the xy-plane by applying a moment of $353t\sin(8\pi t)$ Nm at point O and a moment of $-5000\cos(\frac{3}{2}\pi t)$ Nm at point A, as illustrated by the light gray arrows in Fig. 11. The trajectories of point D in the xy-plane without flow during 0.34 seconds is shown in Fig. 12, and the trajectories in cases where flows of 3 m/s and 6 m/s of concrete through the pipe are modeled. Since the diameter of the pipe and the density of the concrete are homogeneous, the flow speed in kg/s can be readily calculated, and the pressure required to achieve the flow rate can be approximated. From the result we can see that the inclusion of fluid-flow influences the behavior of the fluid-conveying pipe elements, which affects the overall behavior of the robot.

9 Conclusions

Fluid-conveying pipes are part of many flexible multibody systems and can influence the behavior and stability of these systems. Although the development of fluid-conveying pipe elements in the absolute nodal coordinate formulation has gained traction, such elements have not been developed for the widely used floating frame of reference formulation. Therefore the contribution of this paper is fluid-conveying pipe elements, which can be integrated in the floating frame of reference formulation. As such, simulations of flexible multibody systems containing fluid-conveying pipes within this formulation can be conveniently performed.

The fluid is modeled as an incompressible and inviscid plug flow with a prescribed velocity and acceleration. To this end, the pipe is considered as a control volume through which the fluid axially flows. Therefore time differentiation of the position of a material point of the fluid consists of a velocity component stemming from the rigid movement and deformation of the pipe, as well as a component representing the axial velocity of the fluid with respect to the pipe. Through the derivation of the kinematics of material points of the fluid and pipe

and the principle of virtual work, spatial discretization by finite element interpolation functions, and reduction, the equations of motion of the fluid-conveying pipe are derived. The equations of motion can, by the use of Lagrange multipliers, be constrained and combined with other types of elements.

In most implementations of the FFRF, calculation of the volume integrals is avoided through the use of the (lumped) finite element mass matrix. However, the developed fluid-conveying pipe elements contain volume integrals that cannot be approximated using the finite element mass matrix. Therefore a simplification of the elements is proposed. By preimposing deformation upon a straight fluid-conveying pipe element and ensuring that the initial configuration corresponds to the desired stress state by including an additional stiffness term, the behavior of a pipe of arbitrary shape can be approximated. However, if the curvature of the pipe is large, then multiple bodies must be used to model the pipe to meet the assumption of small deformations.

The simplified fluid-conveying pipe elements were validated using the benchmark problems of a straight cantilevered pipe and a curved pipe constrained at one end by a hinge. The results show that the proposed fluid-conveying pipe elements yield similar results compared to the established pipe elements in the ANCF in Spacar. Furthermore, a concrete printing system was modeled, which successfully demonstrated the straightforward integration of the fluid-conveying pipe elements in mechanical multibody systems. As such, this paper provides a definition for fluid-conveying pipe elements within the floating frame of reference formulation, which yields results of similar precision compared to the ANCF and can be combined with elements of different types to simulate larger multibody systems that contain fluid-conveying pipes.

Acknowledgements The authors would like to express their gratitude to Jaap Meijaard for providing the validation data of the straight and curved pipes from Spacar. Furthermore, we would like to acknowledge the financial help coming from the project Smart PrEcise CollaboraTive Robotics for Additive manufacturing of concrete (SPECTRA), funded by Sectorplan project Robotics.

Author contributions K. developed the content of the paper, performed the simulations required for the validation and wrote the main manuscript. M.I. and J. supervised the work and reviewed the manuscript.

Data Availability No datasets were generated or analysed during the current study.

Declarations

Competing interests The authors declare no competing interests.

References

1. Païdoussis, M.P.: Fluid-Structure Interactions: Slender Structures and Axial Flow, vol. 1. Academic Press, London (1998)

2. Zhou, K., Yi, H.R., Dai, H.L., Yan, H., Guo, Z.L., Xiong, F.R., Ni, Q., Hagedorn, P., Wang, L.: Nonlinear analysis of L-shaped pipe conveying fluid with the aid of absolute nodal coordinate formulation. Nonlinear Dyn. **107**, 391–412 (2022)
3. Li, Y., Li, Y., Wen, H., Ning, W.: Dynamical response of a rotating cantilever pipe conveying fluid based on the absolute nodal coordinate formulation. J. Mech. **37**, 359–372 (2021)
4. Balaji, A., Thani, A., Biswas, S., Vyasarayani, C.P.: Stability of a cross-flow heat-exchanger tube with asymmetric supports. J. Comput. Nonlinear Dyn. **17**(11), 111009 (2022)
5. Tang, S., Sweetman, B.: A geometrically-exact momentum-based nonlinear theory for pipes conveying fluid. J. Fluids Struct. **100**, 103190 (2021)
6. Meijaard, J.P.: Fluid-conveying flexible pipes modeled by large-deflection finite elements in multibody systems. J. Comput. Nonlinear Dyn. **9**, 011008 (2014)
7. Hyvärinen, J., Karlsson, M., Zhou, L.: Study of concept for hydraulic hose dynamics investigations to enable understanding of the hose fluid–structure interaction behavior. Adv. Mech. Eng. **12**(4), 1–18 (2020)
8. Wang, L., Ni, Q.: Vibration of slender structures subjected to axial flow or axially towed in quiescent fluid. Adv. Acoust. Vib. **2009**, 432340 (2009)
9. Bauchau, O.A.: Flexible Multibody Dynamics. Springer, New York (2011)
10. Cammarata, A., Pappalardo, C.M.: On the use of component mode synthesis methods for the model reduction of flexible multibody systems within the floating frame of reference formulation. Mech. Syst. Signal Process. **142**, 106745 (2020)
11. Craig, R.R., Bampton, M.C.C.: Coupling of substructures for dynamic analyses. AIAA J. **6**(7), 1313–1319 (1968)
12. Herting, D.N.: A general purpose, multi-stage, component modal synthesis method. Finite Elem. Anal. Des. **1**(2), 153–164 (1985)
13. Rubin, S.: Improved component-mode representation for structural dynamic analysis. AIAA J. **13**(8), 995–1006 (1975)
14. Bathe, K.J.: Finite Element Procedures, 2nd edn. Prentice Hall, Watertown (2014)
15. Wriggers, P.: Nonlinear Finite Element Methods. Springer, Berlin (2008)
16. Crisfield, M.A.: A consistent co-rotational formulation for non-linear, three-dimensional, beam-elements. Comput. Methods Appl. Mech. Eng. **81**(2), 131–150 (1990)
17. Ellenbroek, M., Schilder, J.: On the use of absolute interface coordinates in the floating frame of reference formulation for flexible multibody dynamics. Multibody Syst. Dyn. **43**, 193–208 (2018)
18. Ibrahim, R.A.: Overview of mechanics of pipes conveying fluids—part I: fundamental studies. J. Press. Vessel Technol. **132**(3), 034001 (2010)
19. Farokhi, H., Tavallaeinejad, M., Païdoussis, M.P.: Geometrically exact dynamics of cantilevered pipes conveying fluid. J. Fluids Struct. **106**, 103364 (2021)
20. Chen, W., Zhou, K., Wang, L., Yin, Z.: Geometrically exact model and dynamics of cantilevered curved pipe conveying fluid. J. Sound Vib. **534**, 117074 (2022)
21. Stangl, M., Gerstmayr, J., Irschik, H.: A large deformation planar finite element for pipes conveying fluid based on the absolute nodal coordinate formulation. J. Comput. Nonlinear Dyn. **4**(3), 031009 (2009)
22. Pieber, M., Ntarladima, K., Winkler, R., Gerstmayr, J.: A hybrid arbitrary Lagrangian Eulerian formulation for the investigation of the stability of pipes conveying fluid and axially moving beams. J. Comput. Nonlinear Dyn. **17**(5), 051006 (2022)
23. Yuan, J.-R., Ding, H.: Dynamic model of curved pipe conveying fluid based on the absolute nodal coordinate formulation. Int. J. Mech. Sci. **232**, 107625 (2022)
24. Jonker, J.B., Meijaard, J.P.: A geometrically non-linear formulation of a three-dimensional beam element for solving large deflection multibody system problems. Int. J. Non-Linear Mech. **53**, 63–74 (2013)
25. Humer, A., Steinbrecher, I., Vu-Quoc, L.: General sliding-beam formulation: a non-material description for analysis of sliding structures and axially moving beams. J. Sound Vib. **480**, 115341 (2020)
26. Irschik, H., Holl, H.J.: The equations of Lagrange written for a non-material volume. Acta Mech. **153**, 231–248 (2002)
27. Shabana, A.A.: Dynamics of Multibody Systems. Cambridge University Press, Cambridge (1998)
28. Nikravesh, P.E.: Understanding mean-axis conditions as floating reference frames. In: Ambrósio, J.A.C. (ed.) Advances in Computational Multibody Sytems. Computational Methods in Applied Sciences, vol. 2, pp. 185–203. Springer, Dordrecht (2005)
29. Haug, E.J.: Computer-Aided Kinematics and Dynamics of Mechanical Systems Volume I: Basic Methods. Allyn & Bacon, Needham Heights (1989)